Chapter 9

Extreme Sea Level Projections

Authors: Lucy Bricheno[2], Heather Cannaby[2], Tom Howard[1]

Met Office and CSIRO internal reviewers: Kathleen McInnes[3], Matthew Palmer[1]

1 - Met Office, Exeter, UK

2 - National Oceanography Centre, Liverpool, UK

3 - CSIRO, Australia

Contents

9.1 Introduction

Given its considerable population, industries, commerce and transport located in coastal areas at elevations less than 2 m (Wong, 1992), Singapore is particularly vulnerable to changes in extreme sea levels.

Changes in extreme sea levels arise through some combination of: (i) changes in time-mean regional sea level; (ii) changes driven by regional processes that control the most extreme sea levels, which are often linked to local meteorology. Changes in time-mean regional sea level have been presented in Chapter 8. This work in this chapter explores potential changes in waves and surge activity for the Singapore region, under climate change. The results presented are based on the RCP8.5 scenario, which is the most severe emissions scenario used in the IPCC 5th Assessment Report (hereafter "AR5"). The scientific background to changes in sea level extremes for the Singapore region has been presented in the previous Chapter 8 report. In Section 9.4.2 of this chapter we present our recommended method to combine mean sea level projections (Chapter 8) with surge projections (this chapter) and present day extreme sea level data, to produce site-specific projections of extreme sea level for the 21st Century.

Subannual variations in water levels around Singapore are controlled by a combination of tidal and atmospheric effects. The typical tides are mixed diurnal and semi-diurnal with a range around 2-3 m, but are regular and predictable. Extreme sea levels are generated by wave and surge events – driven by low atmospheric pressures and strong winds. Large wave events are associated with monsoon winds, and peak twice per year during the northeast monsoon (December – February) and the southwest monsoon (June – August). The Singapore hydrograph department reports waves of order 1 m high along the South West coast. High sea levels occur during the northeast monsoon, due to wind set-up, while water levels are depressed during the southwest monsoon due to set down. This leads to a seasonal cycle in mean sea level with an amplitude of around 20-30cm. Extreme sea level anomaly events in Singapore tend to coincide with prolonged (lasting for several days) NE winds over the South China Sea occurring during the winter monsoon season (e.g. Tkalich et al., 2009). Very rarely, tropical cyclones move close to the equator. There is one recorded case of a cyclone impacting Singapore during December 2001. Tkalich et al (2009) suggest that this event did not result in an extreme sea level anomaly event at Singapore. Therefore, tropical cyclones are unlikely to be an important factor for extreme sea level in the region of interest.

The outputs from regional climate model (RCM) experiments (Chapter 5) have been used to drive high resolution (12 km) storm surge and wave models around Singapore to study the effect of changes in atmospheric storminess on local water levels. This dynamic downscaling approach has been successfully applied in the past, for e.g. UKCP09 (Lowe et al. 2009) and CLASIC (Farquharson et al., 2007). The models used in this downscaling report were chosen to have a reasonable representation of present climate, and also to cover the largest range of possible future responses. For example, GFDL-CM3 showed the strongest change in the strength of the northeast monsoon. In this chapter, phrases like "HadGEM2-ES" are routinely used as shorthand for "the RCM simulation with HadGEM2-ES boundary conditions".

The layout of the document is as follows. Section 9.2 outlines the models used to simulate waves and surges in the Singapore region, and describes the statistical and analytical methods used to evaluate the model outputs. Section 9.3 presents an overview of the data products used at the model validation stage. Section 9.4 contains results from the tide-surge model (9.4.1) and wave model (9.4.3). These were broken down by seasonality and the individual driving RCM, then the extremes were considered and in some cases combined to give a mean and a range. Section 9.5 summarises the main findings and Section 9.6 points to our key recommendations on how to use the findings of this chapter, and lays out some caveats to the results.

9.2 Methodology

For both wave and surge models, bathymetry is derived from the General Bathymetric Chart of The Oceans (GEBCO, http://gebco.net), and linearly interpolated onto a regular latitude-longitude grid at 1/12th degree (~10 km) resolution.

Downscaled simulations of wave and surge are performed using forcing sets generated from RCM simulations, undertaken as part of Chapter 5. These RCM simulations are downscaled from the following CMIP5 (Taylor et al., 2012) global climate models (GCMs): HadGEM-2ES, GDFL-CM3, CNRM-CM5, IPSL-CM5A-MR. These models were selected to best span the range of monsoon circulation responses, which is likely an important driver of both surge and wave changes, as discussed in Chapter 3. We were also constrained in our choice by the availability of high-frequency parent-GCM forcings to drive the global wave model (used as open boundaries for the regional wave model).

Hourly mean sea level pressure (SLP), and 10 m wind speed from the regional climate models are used as inputs to the surge model. The wave model is forced by hourly 10 m wind speeds. For each climate model simulation we present a historical mean state, based on the 1970-2009 time slice. Three further time slice simulations are then presented (for each of the four GCM models) focusing on each time horizon in turn: reflecting early (2009-2039), mid (2039-2069) and late century (2060-2099) change.

All surge model simulations are run one year at a time. Each year is spun-up for a five day period. Using a short spin-up period for the surge modelling is a reasonable approach, as there is little ‘memory’ in this system. The storms responsible for large surge and wave events are short acting, so only require a spin-up time of a few days at most. The surge model is run for a period from June to June, so that the spin-up is less likely to over-lap with extreme events which are most prevalent during the winter monsoon period. The RCMs also have different calendars, for example GFDL-CM3 uses a 365-day calendar, while HadGEM2-ES uses a 360-day model year. The wave model is run continuously, with warm-starts at the beginning of every year (in other words the starting conditions of one year are taken from the finishing conditions of the previous year).

Table 9.1: CMIP5 models used, and their calendars

Model name	Calendar year
CNRM-CM5	Gregorian
HadGEM2-ES	360 days
GFDL-CM3-CM3	365 days
IPSL-CM5A-MR	365 days

9.2.1 Surge model

The Nucleus for European Modelling of the Ocean (NEMO, www.nemo-ocean.eu, Madec (2008)) is used to model the surge component. NEMO is configured at a 1/12th degree resolution, covering the region 95 – 117 °E and 10 °S – 17 °S, as shown in Figure 9.1. The model runs with 9 sigma levels in the vertical, logarithmic bottom friction, constant density, a 4-second barotropic time step, hourly SLP and 10 m wind forcing applied using a 'flux formulation' and hourly sea-surface height (SSH) output. Tidal forcing is applied at the open boundary as a time series of sea-surface elevation representing 15 harmonic tidal constituents: Q1, O1, P1, S1, K1, 2N2, MU2, N2, NU2, M2, L2, T2, S2, K2, and M4. Surge generation occurs locally in the model, as a result of mean sea level pressure changes (the inverse barometer effect) and 10 metre winds. By running NEMO as a coupled tide and surge model, tide-surge interactions are also included. The model is also run in a tide-only configuration for the full period, so that a surge residual can be assessed separately. The wave and surge models are run uncoupled from one another, and wave-current interactions will not be considered. The domain of this model is presented in Figure 9.1.

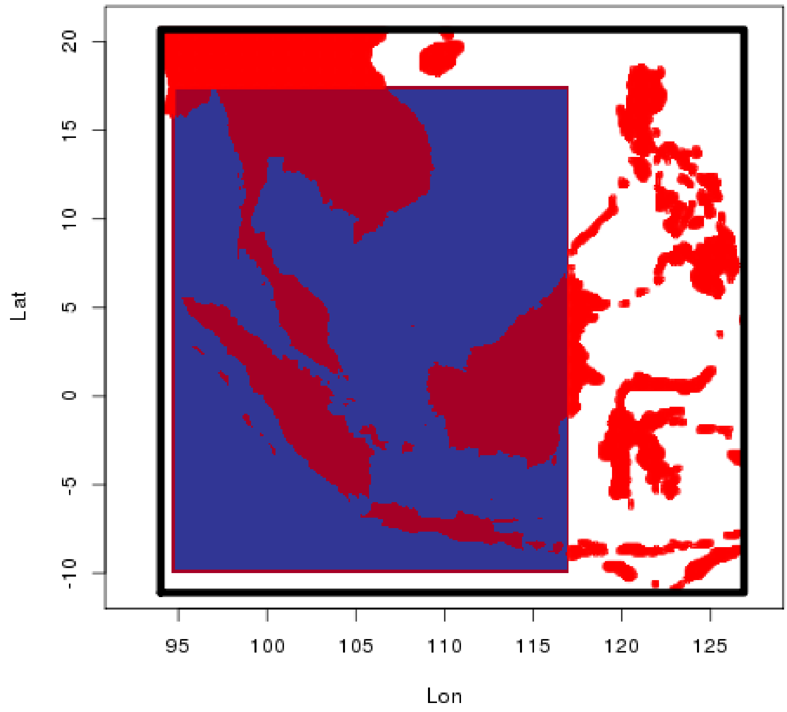

Figure 9.1: Model domains for surge modelling. The NEMO surge model domain is shown in blue with its land mask shown in red. The outer square shows the limits of the regional climate model: land again shown in red, with RCM sea area shown in white.

A storm surge is defined as a short-lived increase in local water level above that of the astronomical tide. Storm surges are driven by atmospheric pressure gradients and winds, with winds being more effective at generating surges in shallow water (Lowe et al. 2009) and in the equatorial region. When they occur near or at high tides, surges are likely to cause flooding. It is important to establish the likely change in frequency of such events in order to maintain a consistent level of protection of livelihoods and infrastructure.

The work presented here follows the approach of studies such as Lowe et al. (2009), who produced a similar assessment for the United Kingdom, and Sterl et al. (2009) who assessed extreme surge changes in the North Sea, a shallow coastal sea off north west Europe. The change in extreme sea level can be separated into a component of change in the sea level extremes due to any changes in atmospheric storminess and a change in regional time-mean sea level (Chapter 8[1]). There is good evidence (Howard et al., 2010; Sterl et al., 2009) that these two components of change can be modelled separately and then combined linearly to give a total projected extreme sea level change.

The principal effect of a positive surge on the tide is to increase the propagation speed and thus bring forward the times of the tidal cycle. Thus peaks in surge residual (defined as the difference between the astronomical tide and the actual water level) are typically obtained prior to the predicted high water (Horsburgh and Wilson, 2007) and are sometimes related merely to timing differences which may have no flooding implications (the high water level may be the same as the astronomical high tide prediction, but simply arrive earlier). A more significant and practical measure than the surge residual is the skew surge (see Appendix 9.2), which is the difference between the elevation of the predicted astronomical high tide and the associated high water during the same tidal cycle (e.g. de Vries et al. 1995). For this reason there is a growing consensus that skew surge is the preferred metric over surge residual (e.g. Howard et al., 2010, Batstone et al., 2013).

9.2.2 Wave model

Wave simulations are performed using a stand-alone Wavewatch III model. WAVEWATCH III ® (Tolman 1997, 1999a, 2009) is a third generation spectral wave model, developed by NOAA and NCEP. The model is configured at a 1/12th degree resolution, covering the region 95 – 117 °E and 9 °S -14 °N. The model bathymetry and domain are plotted in Figure 9.2. In order to capture swell incoming at the open boundaries, a 50 km resolution global wave model was also run (see Appendix 9.3).This was forced by the GCMs listed in Table 1 which correspond to open boundary forcing for the atmospheric RCMs. The model is divided into land and sea points and also a third class of intermediate points where partial blocking is used to transmit wave energy through regions where the sheltering effect of small islands cannot be resolved by the model.

In a spectral wave model, the choice of source terms dictates how the model represents energy input through winds, and dissipation through wave breaking and white capping. Two sets for source terms were tested and compared: WAM cycle 4 (Monbaliu 2000) and Tolman and Chalikov (1996). The latter set is used for the Met Office global wave model but has problems with shorter fetch, which grows slowly and dissipates slowly causing a model bias. WAM cycle 4 has a reduced bias overall but also reduced performance in the tropics. Very little difference was found between these two source

---

[1] Palmer et al. 2014a, Palmer et al. 2014b

terms for the domain of interest and consequently Tolman and Chalikov source terms were chosen due to the quicker integration time better suited to long period runs.

The wave model is forced hourly, with a global time step of 900 seconds. WaveWatch III produces hourly outputs of wave height, mean wave energy period, mean wave direction, mean directional spread and mean wave period. The model was configured with a spectral resolution of 30 frequency bins and 24 directional bins.

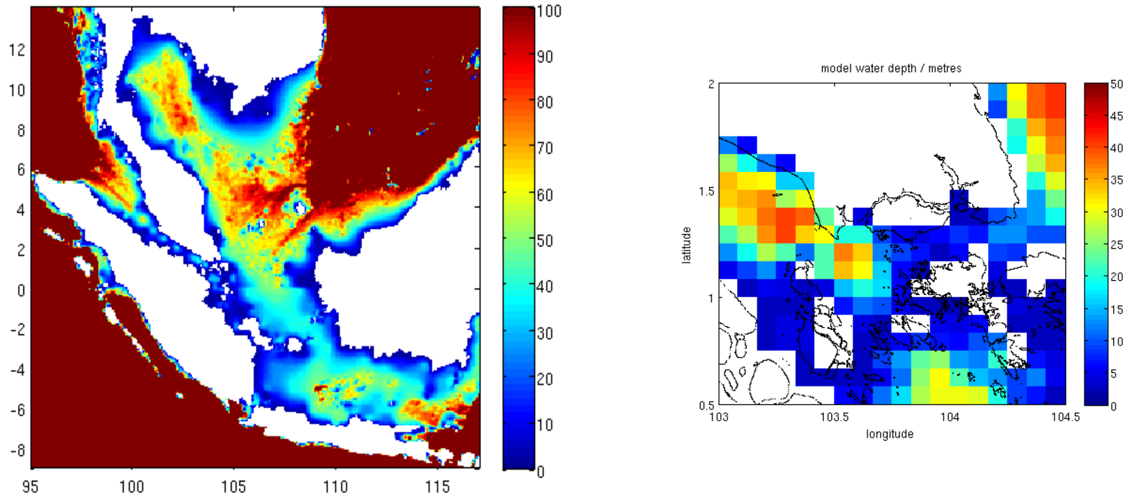

Figure 9.2: Wave model domain and bathymetry in metres (left), highlighting shallow waters, and a close up of the area around Singapore (right).

9.2.3 Extremes Analysis

The worst coastal flooding impacts are experienced during extreme events, for example an extreme high water resulting from a storm surge at high tide, and the accompanying extreme waves. By definition these are rare events, and our ability to simulate them is limited by the length of the model simulation.

To address this limitation, we fit a statistical model to the simulated extreme events. We do this for two reasons: firstly in order to make predictions regarding return periods longer than the period of the simulation, and secondly in order to incorporate many events into our model of the behaviour at any given return period. (This approach is analogous to the way in which a simple linear 'line of best fit' incorporates many observations to identify the relationship between two variables which are believed to be linearly related, facilitating both predictions outside of the observed data, and more robust estimates within the observed range).

The statistical model we use is the generalised extreme value (GEV) distribution (see for example Coles, 2001). There is good theoretical justification for this choice: again an analogy will help. Suppose we have a set of blocks of data (for example, 150 one-year blocks of hourly sea surface elevation). We take the mean of each block. Now we have 150 annual means. Invoking the central limit theorem (CLT) we can argue that we expect this set of 150 values to be well-approximated by a normal distribution, because in creating the 150 values we took a measure (the mean) representative of the centre of each block. We can fit a normal distribution to our set of 150 values and use the two parameters of the normal distribution – the mean and the standard deviation – to make robust statements about the probability of the annual mean exceeding a particular level.

Analogously, suppose we instead take the maximum of each block. Now we have 150 annual maxima. This time invoking the external types theorem (ETT) we can argue that we expect this set of 150 values to be well-approximated by a generalised extreme value (GEV) distribution, because in creating the 150 values we took a measure (the maximum) representative of the extreme of each block. Notice that we expect the maxima to be distributed differently to the means. We can fit a generalised extreme value distribution to our set of 150 values and use the three parameters of the GEV distribution – the location, scale and shape – to make statements about the probability of the annual maximum exceeding a particular level. The location parameter of the GEV is analogous to the mean of the normal distribution – a change simply slides the whole distribution up or down. The scale parameter of the GEV is analogous to the standard deviation of the normal distribution – an increase widens the spread of the distribution, in the case of the GEV moving the long-period return levels further from the short-period return levels. Thus a change in either parameter can affect the long-period return levels. In this work we consider the century-scale change in both location and scale.

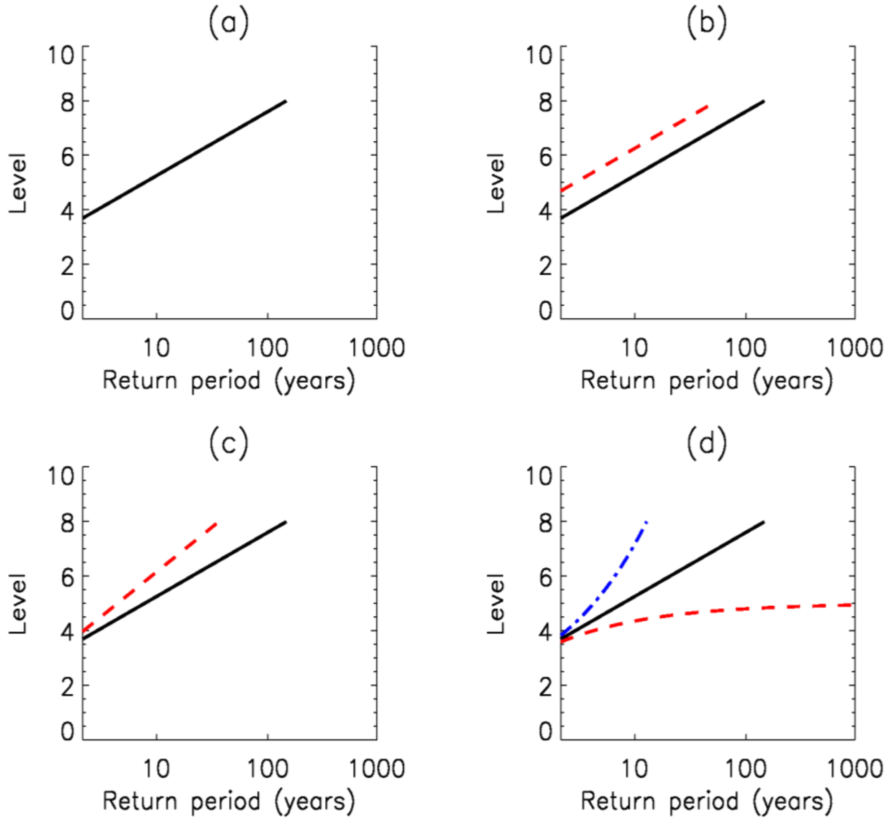

Figure 9.3: Schematic illustrating the effect of the three parameters of the GEV distribution on a return level plot. (a) The Gumbel distribution (shape=0) appears as a straight line on the return level plot. (b) Increasing the location parameter shifts the whole distribution to higher levels (dashed red line). (c) Increasing the scale parameter increases the gradient of the line, pushing the rare extreme return levels higher but having little effect on the more frequently observed events (dashed red line) (d) The shape parameter affects the curvature of the return level plot. The dashed red line shows a distribution with a negative shape parameter. The dot-dash blue line shows a distribution with a positive shape parameter.

The impact of the shape parameter is most readily seen by considering a return period curve (e.g. Figure 9.3). In this work, consistent with previous work such as UKCP09, and consistent with expert advice (Tawn, pers. comm.), although we fit the shape parameter to our simulated extremes, we do not consider century-scale change in the shape parameter, but rather we assume that it remains constant for a given simulation. Thus we allow for the fact that we do not have a theoretical basis for constraining the shape parameter (which might be done for example by choosing the Gumbel distribution, which has a shape parameter of zero).

An important caveat is that both CLT and ETT arguments involve underlying assumptions of independence. Strictly we require that the behaviour of the extremes in one year is independent of the behaviour of the extremes in neighbouring years. There is large inter-annual variability in both the modelled and observed extreme water levels, which can make any long-term trends difficult to identify against the background of natural variability. Thus the function of using a fitted GEV distribution is to make a robust assessment of these century-scale trends. The GEV distribution was fitted to the modelled extreme skew surges and wave heights during the 1970-2099 period. Note that the long-term mean sea level was not varied in the wave and storm surge model; this part of the assessment was concerned with century-scale changes arising from changes in atmospheric storminess only.

We tested the impact of using the R largest events (R ranging from 1 to 5) each year instead of just the annual maxima (subject to a separation of at least 120 hours in an effort to ensure independence). Our overall result is not strongly sensitive to this change.

Allowing the location parameter to change accommodates potential change in all extreme events (for example at both long and short return periods). Allowing the scale parameter to change accommodates the potential for an increase (or decrease) in the spread of extreme surges (for example an increase in intensity of the most extreme surges accompanied by a decrease in intensity of the more frequent surges). A comparison of the quality of the stationary and non-stationary fits gives an indication of the significance of any trend which is seen.

The analysis is performed using R statistical package. Literature on application of the GEV method can be found in Coles (2001), Hosking et al. (1985), Huerta (2007), Katz et al. (2002), Méndez et al. (2007), and Méndez et al. (2006).

9.3 Data

The tide surge and wave models are forced by high resolution regional climate models (RCMs), run at approximately 12 km resolution. In order to assess the level of storminess in the climate models, a 95th percentile of hourly winds is extracted from each of the 4 RCMs (see Appendix 9.1). This gives context for the potential differences between the downscaled models. The four models used in the downscaling work show some consistent differences looking at 1970-1999 vs. 2070-2099. Slower winds are predicted to the southwest of Sumatra and in some cases (e.g. CNRM-CM5) in the Malacca Strait itself. Faster winds are observed around Singapore and into the South China Sea. The strongest positive change is observed in the IPSL-CM5A-MR model.

In order to evaluate the models, a hindcast period was simulated. Both wave and surge models were forced by ERA-40 data for the period 1985-2005. The model outputs were then validated against observations from tide gauges in the case of NEMO and satellite wave observations in the case of WaveWatch III for real events. Tide gauge data were available at Bukom, Cafhi Jetty, Lim Chu Kang, Raffles Light House, Sembawang, Sultan Shoal, Tanah Merah, Tanjong Pagar, Ubin, West Coast, West Jurong Tuas and West Tuas (Figure 9.4).

Figure 9.4: Map of tide gauge locations used for model validation

The wave model was validated against satellite observations from EnviSat (Atlas et al. 2011), and an example plot of the data coverage is given in Figure 9.5. Although there is a wave buoy in the Johor Strait (01°20' 39.585''North, 104°04' 51.0398 East), which collected data during 2003-2008, this location is not represented by a 'wet-point' in WaveWatch III, so could not be used directly for validation.

9.3.1 Tide and Surge Model Validation

Maren (2012) examine the tides close to Singapore, finding tides in the coastal waters to be complex, mixed between diurnal and semi-diurnal. This section briefly examines the model performance in terms of its representation of tides & surges. The leading tide constituents (M2, N2, N4, M4, and K2) are well captured but the secondary mode diurnal components (K1, O1, P1) are slightly over predicted in the model. As we are concerned with extreme water levels in this study, it is considered adequate to well represent the tidal range, and NEMO is found to well-capture both the magnitude and phase of the largest tides. Figure 9.6 shows a strong spring-neap cycle, and good agreement between model and observations, particularly for the maximum water levels.

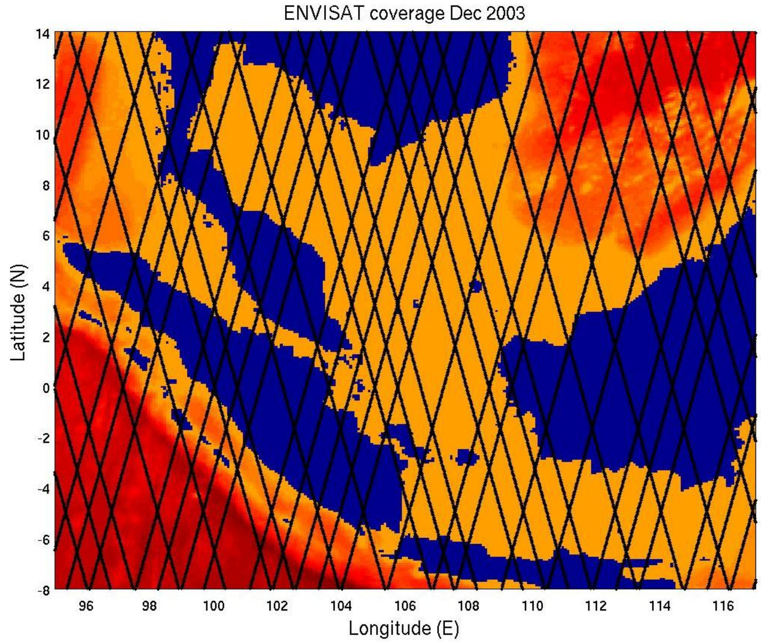

Figure 9.5: Tracks of EnviSat coverage during December 2003

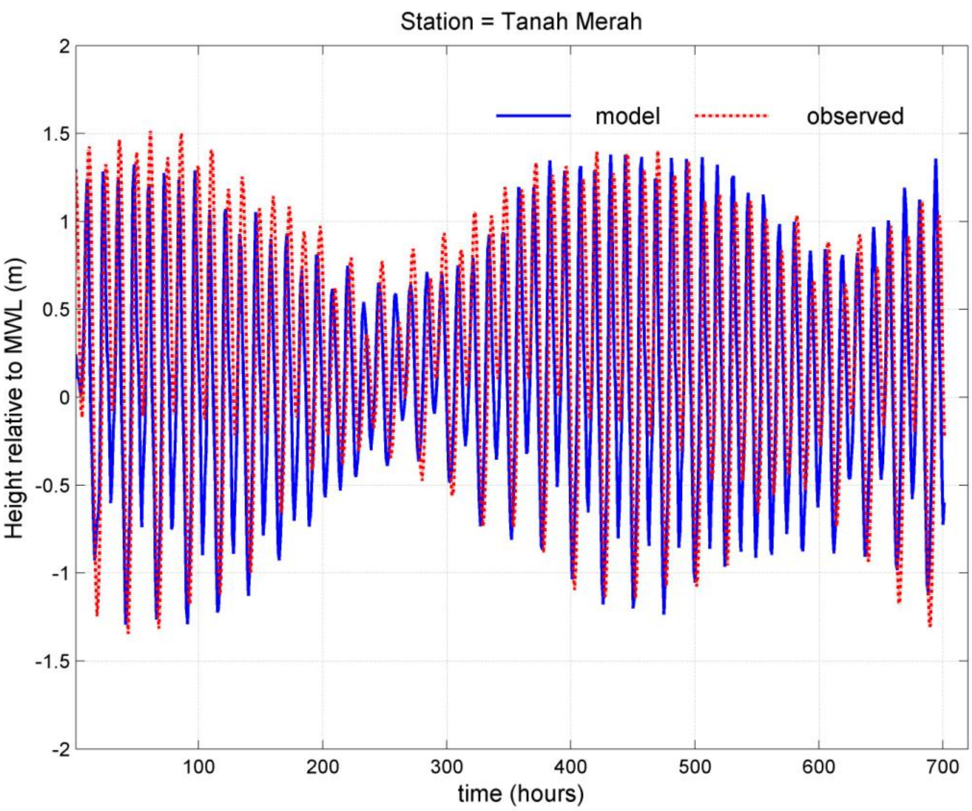

Figure 9.6: Comparison of observed and modelled water levels at Tanah Merah during February 2003.

Harmonic analyses of modelled and observed sea surface heights were performed using T_TIDE (Pawlowicz et al, 2002) and tidal amplitudes and phases were then compared. Some of the Malaysian tide gauges located close to Singapore: Kukup, Keling, Lumut were also analysed. Tidal amplitudes (see Figure 9.8) were well captured, particularly the dominant semi-diurnal constituents. The diurnal components which are largely responsible for the secondary peak observed in tidal time series are less well captured by the NEMO model. A comparison of tidal phases is presented in Figure 9.7. Further tide-surge model validation related in particular to the simulation of extreme water levels is presented in Appendix 9.10, where it is shown that the scale parameter in particular is well modelled. In our recommended method for producing site-specific projections, this parameter is the critical one for estimating changes in the magnitude of the most extreme surge events.

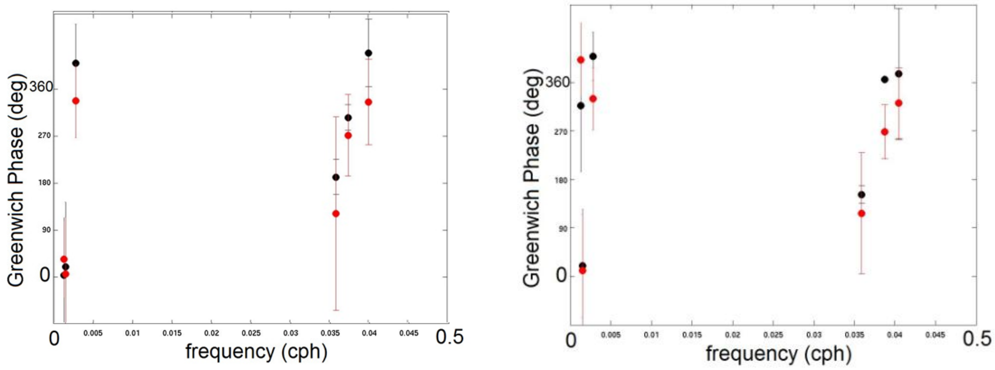

Figure 9.7: Comparison of modelled and observed tidal phases at Tanah Merah (left) and Kukup (right). Tidal phase angles with 95% Confidence Interval (black = observations; red = model).

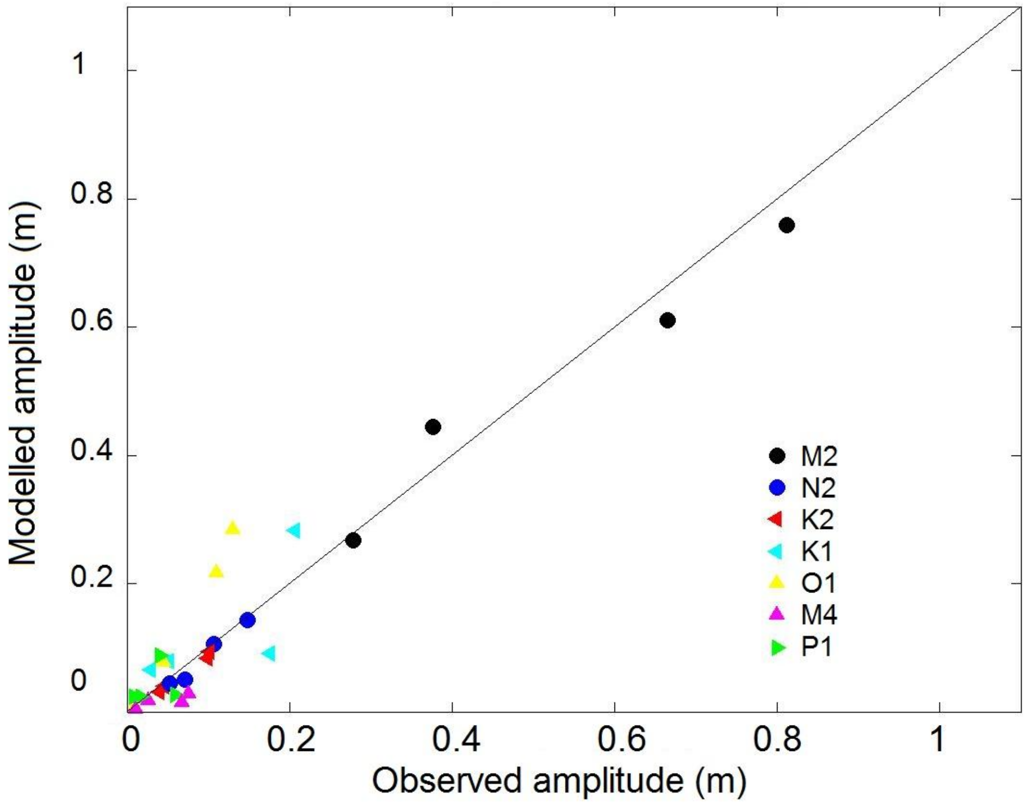

Figure 9.8: Comparison of modelled and observed tidal amplitudes at several sites close to Singapore: Stations Keling, Tanah Merah; Lumut; Kukup.

9.3.2 Wave Model Validation

Modelled significant wave height (Hs) was compared to along-track significant wave height derived from ENVISAT altimetry data (These data were obtained via the Globwave data portal (http://globwave.ifremer.fr/)). Point-to-point comparisons were made between individual satellite data points and the nearest model grid point. All satellite data available within the model domain between 2003 and 2005 were used for this analysis.

When points across the whole domain, for the validation year 2003 are compared against Envisat, the wave model has a mean correlation coefficient of 0.85, and a small standard deviation of around 0.52 m, an RMSE of 0.53 m, and a mean bias of -0.11 m. A high correlation coefficient signifies good agreement with observations, while a small standard deviation and small RMS indicate low errors. The results presented here compare well with the UK Met Office's operational wave model, which has a standard deviation of around 0.8 m and a correlation coefficient of 0.82 (Bidlot et al. (2002), Bidlot et al. (2007), Bidlot & Holt (2006)). This model standard deviation is low when compared to the Met Office model value of 0.8 m, however their wave model covered the North Atlantic, where wave heights are large in comparison to our study area.

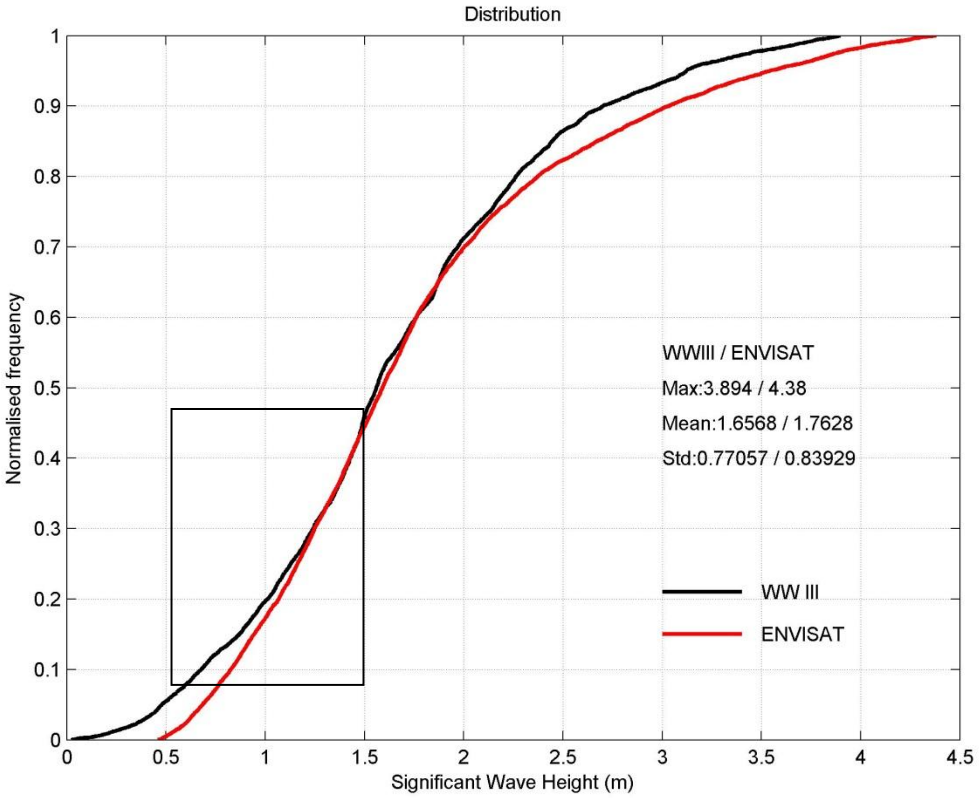

Figure 9.9: Comparison of modelled significant wave height (Hs) with that observed by EnviSat throughout whole model domain during 2003. Typical wave heights around Singapore fall within the boxed region.

Figure 9.9 presents WaveWatch III validation: wave heights are under-predicted at high Hs, and Envisat is unreliable at low waves (Hs < 0.5m). Some under-prediction is seen at large wind speeds/wave height (Hs >2 m).This plot is for the whole wave model domain. Typical Hs around Singapore is around 0.5-1 m, in the range at which the wave model is performing at its best.

9.4 Results

9.4.1 Tide and Surge Model Results

Storm surges and tides are shallow water waves, i.e. their wavelength is much greater than the water depth, since they have typical horizontal length scales of hundreds of kilometres. In terms of this length scale, Singapore is a small island. The real-world tide and surge will be modified by details of the coast and bathymetry which are not resolved in our model (one example being the Johor Strait, which does not appear on the scale of the model). The value of the surge model is in the use of atmospheric data downscaled from the climate model simulations to make projections of century-scale trend in extreme surge events in the Singapore region (not in making specific localised operational surge forecasts). In order to diagnose the surge trends, then, we analyse a single point close to Singapore (Point ‘a’ in Figure 9.12), which we take to be representative of the large scale surge signal for the whole region. Support for this approach is shown in Figure 9.11 and further in Appendix 9.8, which shows how closely-related neighbouring points are. Spatial variations are discussed further in section 9.6.

Time series of annual maximum skew surge from each of the four climate model simulations considered are presented in Figure 9.10. For each simulation we quote the P-value associated with the model improvement moving from a stationary to a non-stationary model. There will always be some model improvement because we are adding more parameters to the model (i.e. a linear time-variation in both location and scale). Taking the CNRM model as an example, the P-value is 77%. This means that if we were to generate many samples of random stationary data with the GEV parameters of the stationary fit, and then fit a non-stationary model to the results, we would expect a greater improvement in fit than that seen in the CNRM data in 77% of cases. In simple terms, the small amount of apparent non-stationarity in the CNRM data could easily arise by chance from random variations in stationary data. Thus we cannot discount our null hypothesis that the CNRM data is stationary in time. For the IPSL model, on the other hand, consistent with the visual impression given by the plot, the P-value is very small and we conclude that this data is unlikely to be stationary. Visually, there is a strong suggestion in the IPSL data of a reduction in variability over the 21st century.

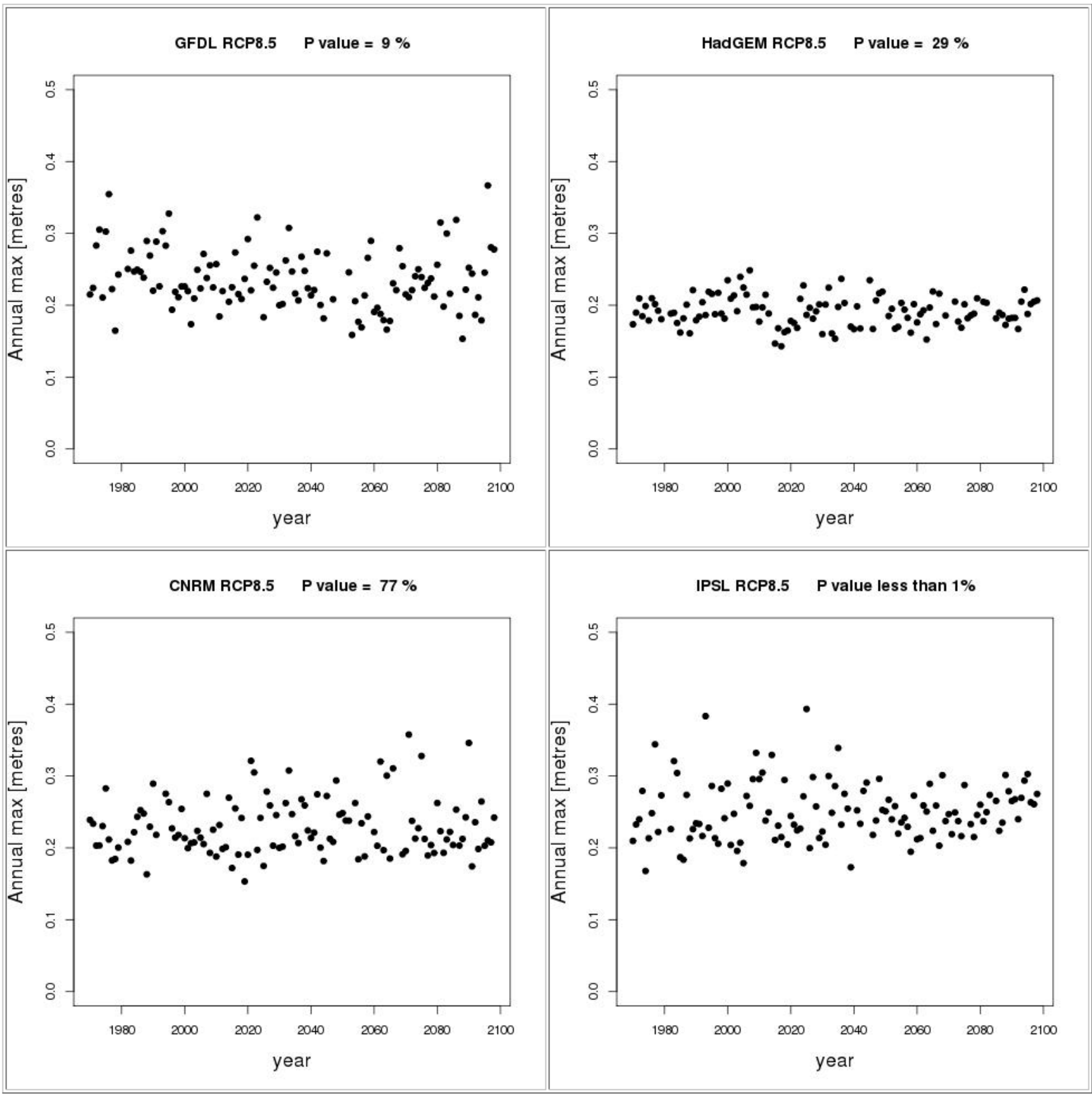

Figure 9.10: Simulated annual maxima of skew surge (metres). A consistent scale on the Y-axis is used across all four models for ease of comparison. The P-value indicates the statistical significance of the improvement in fit when we use a non-stationary GEV model: large P-value indicates little improvement, small P-value indicates significant improvement. See section 9.2.1 for a discussion and Appendix 9.2 for a description of the skew surge metric.

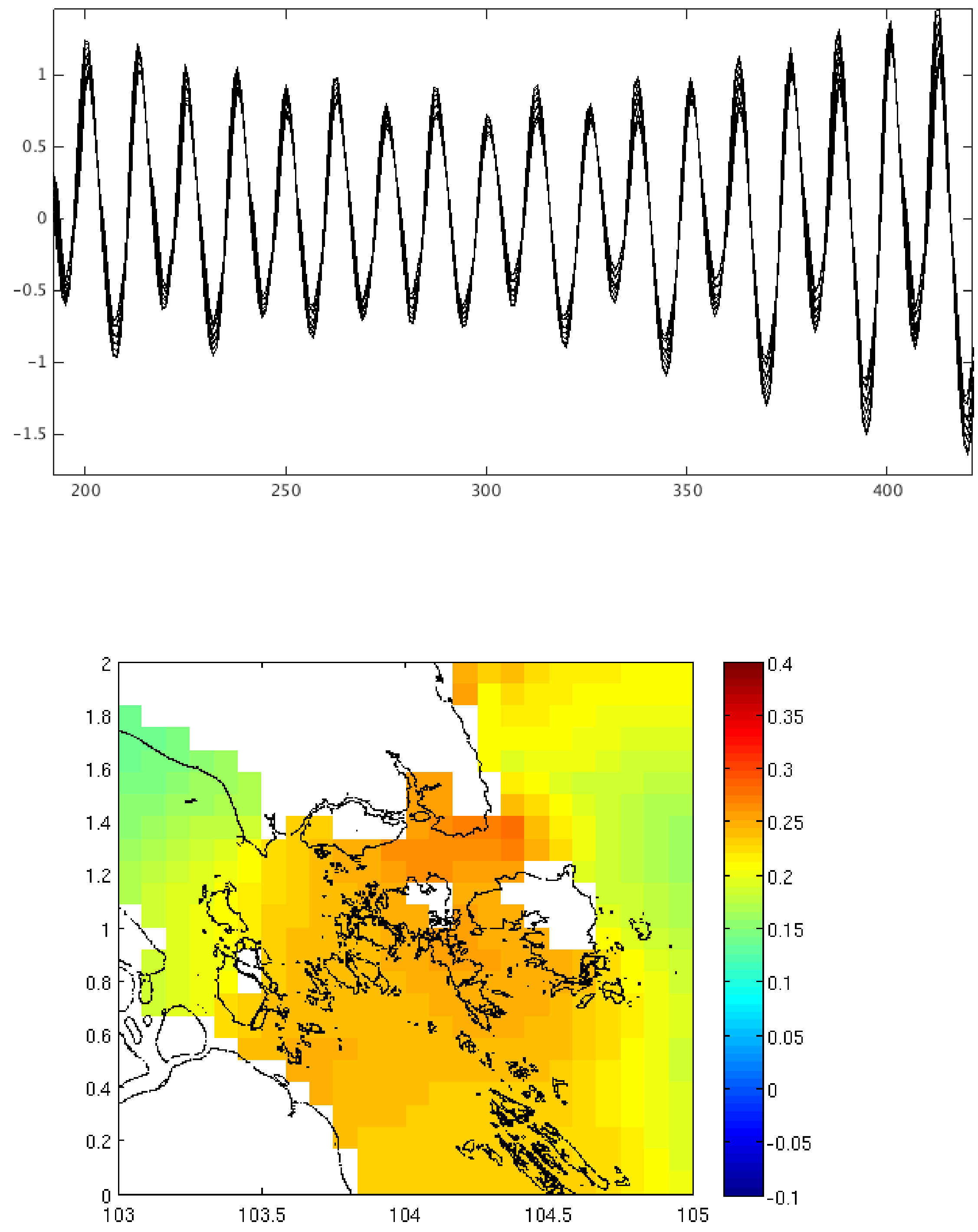

Figure 9.11: (Top) typical approximate 200-day time series showing water levels (units: metres) at the 13 active points around Singapore (see next figure for locations) (bottom) and a map showing the smoothly varying surge residual, taken from an event during the ERA40 simulation (units: metres).

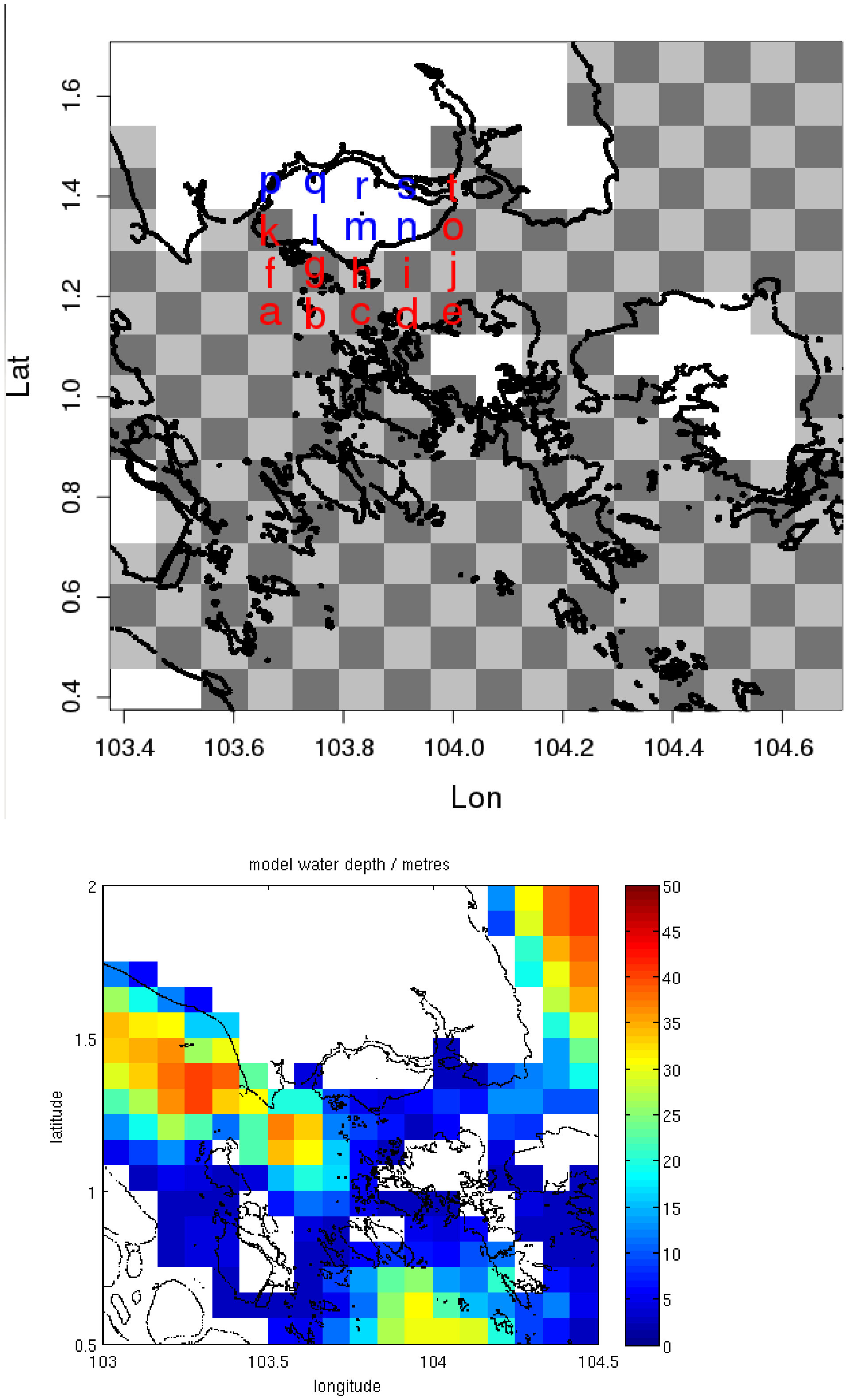

Figure 9.12: Top: detail of surge model grid around Singapore with grid point identification letters a-t. The 'chequerboard' in two shades of grey shows active (sea) grid cells. White shows land cells (thus letters l, m, n, p, q, r, and s are inactive (land) cells). Bottom: modelled water depths on the WW3 grid (metres). The NEMO surge grid has more active points than the WW3 grid.

HadGEM2-ES

To illustrate our approach we present results of the NEMO simulation forced by HadGEM2-ES under RCP8.5 for grid point ‘a’ (see Figure 9.12 for grid point locations). Analogous results for the other three models are shown in Figure 9.10 and Appendix 9.6. First we consider the time series of the annual maximum skew surges for the NEMO simulation driven by HadGEM2-ES, as shown in Figure 9.10 (top right panel) and reproduced in Figure 9.13 for ease of reference.

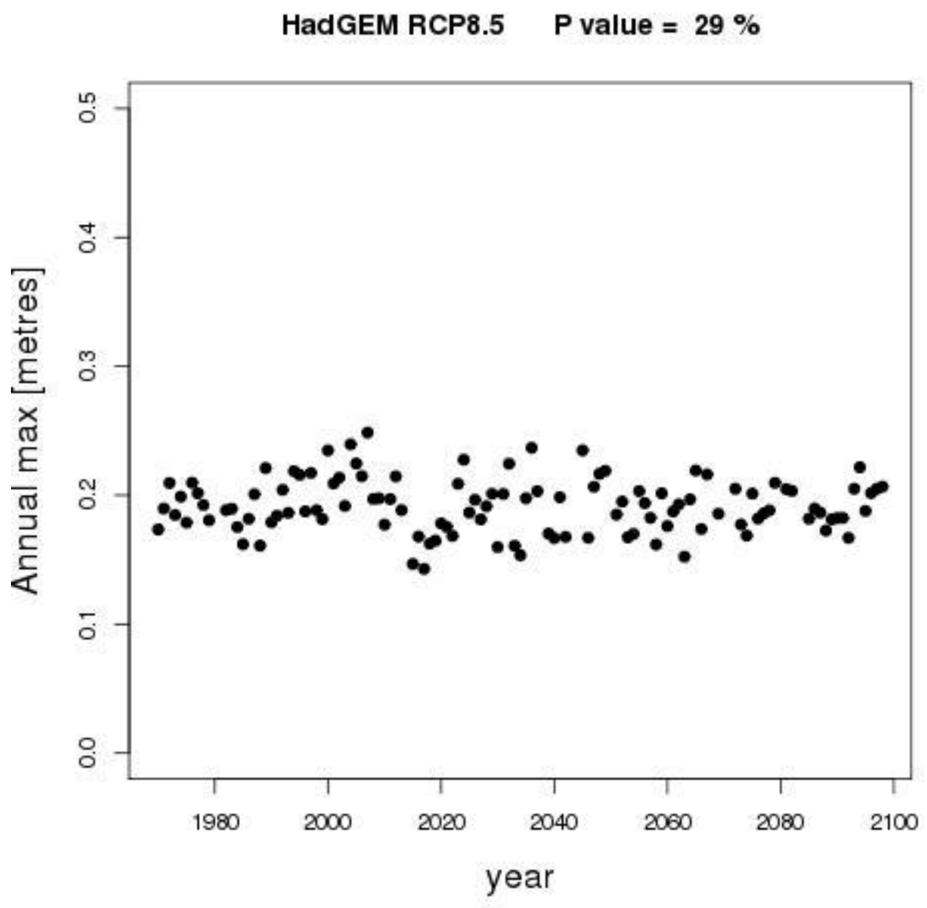

Figure 9.13: Time series showing the annual maximum skew surges (metres) for the NEMO simulation driven by HadGEM2-ES.

Posing a null hypothesis that all years are drawn from the same underlying extreme value distribution, we fit a stationary GEV distribution to the data. Standard diagnostic plots of the quality of this fit are shown in Figure 9.14; we regard the quality of fit to be good enough to justify proceeding with the analysis.

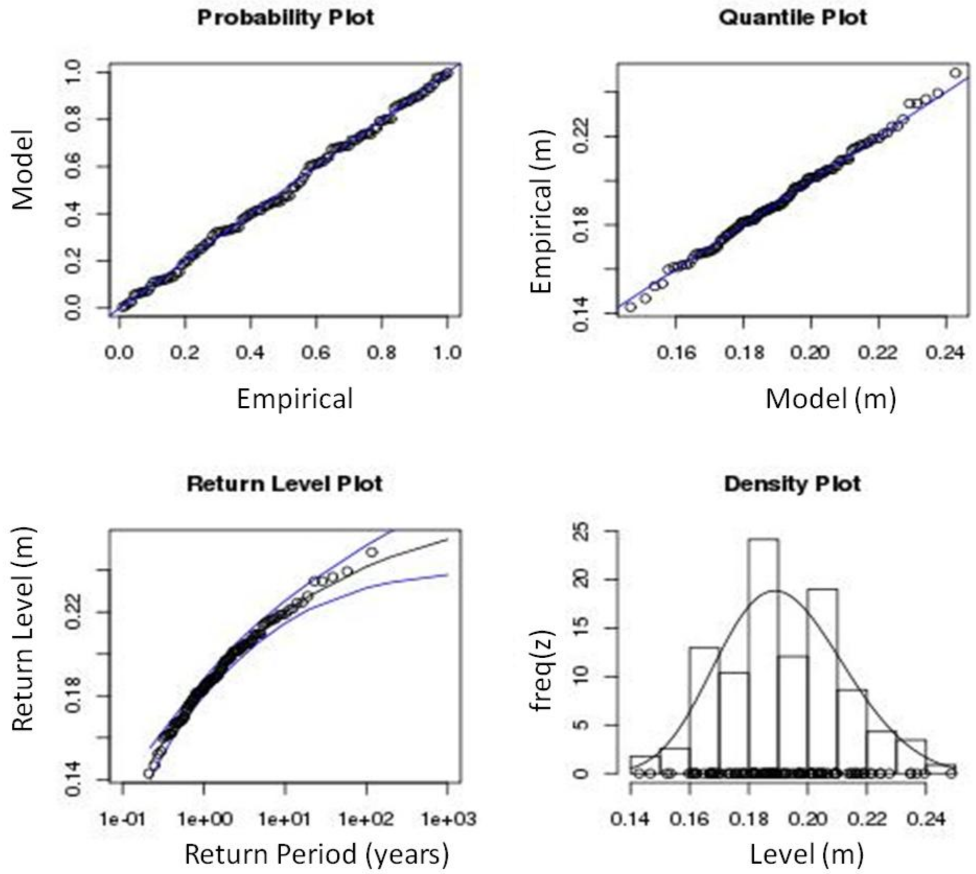

Figure 9.14: Standard diagnostic plots for the GEV stationary fit to the HadGEM2-ES skew surge data. All four plots give an indication of the quality of fit of the GEV model to the data. In each case the fit is quite acceptable. For further details of how to interpret these plots see Coles (2001).

Next we test a hypothesis that the extremes shown in Figure 9.13 come from a non-stationary distribution with both location and scale changing linearly with time over the period 1970-2100. Inspection of Figure 9.13 does not strongly suggest this hypothesis and nor does the standard measure of the improvement of fit, the P-value, which is around 29%. Thus this alternative hypothesis is not well-supported by the data. Consistent with its statistical insignificance, the calculated trend in, for example, the 100-year return level is physically small: about minus 19 mm per century.

For each model, from the non-stationary fit we can diagnose a linear century-scale trend in return level associated with any given return period. In order to produce trends and uncertainties which are representative of the four models taken as a whole, for any given return period we take the four central estimates of trend (one from each model) and identify the mean of these four (μ) as our small-ensemble central estimate and the (Bessel-corrected) standard deviation of these four (σ) as the uncertainty. We then identify (μ - 1.64 σ) as our lower bound and (μ + 1.64 σ) as our upper bound. We do this in order to inflate the uncertainty given by the model range, in recognition of the small ensemble size (4 models). We note that this approach is different to that of the atmospheric chapters. Although the chosen factor of 1.64 is consistent with the 5th and 95th percentiles of a normal distribution, this does not mean that the four results should be assumed to have been drawn from an underlying normal distribution, or indeed any other form of distribution. Therefore, we do not identify the lower and upper bounds with any quantified level of risk, consistent with the approach described in the atmospheric work. Our lower and upper bounds are simply one way (by no means the only possible way) to compensate approximately for the small ensemble size, in the absence of any further information. Furthermore, we note that (1) this approach is broadly consistent with the approach to the surge component taken in UKCP09 (Lowe et al, 2009) and (2) our end result (the total uncertainty in projected change in extreme sea level) is not sensitive to this choice, because the uncertainty in the total change is dominated by the uncertainty in mean sea level change, with the surge change uncertainty a relatively minor component.

Following this procedure we obtain century-scale trends in skew surge component as shown in Table 9.2. These values are illustrated in Figure 9.15. For other return periods, interpolation between the points in Figure 9.15 is acceptable. As stated previously, we tested the impact of using the R largest events (R ranging from 1 to 5) each year instead of just the annual maxima. Our overall result is not strongly sensitive to this change, and furthermore for some simulations (in particular GFDL and IPSL) the parameter estimates do not remain stable as R increases, and so the use of R>1 cannot be justified for those simulations. Thus for consistency we selected R=1 (annual maxima only) for all four simulations.

Table 9.2: Projected century-scale trends in skew surge for five return periods due to storminess changes only (i.e. excluding mean sea level change) (metres per century, to two decimal places)

Period/years	2	20	100	1000	10000
Lower	-0.02	-0.04	-0.06	-0.09	-0.12
Central	0.00	-0.01	-0.02	-0.02	-0.03
Upper	0.02	0.02	0.03	0.05	0.06

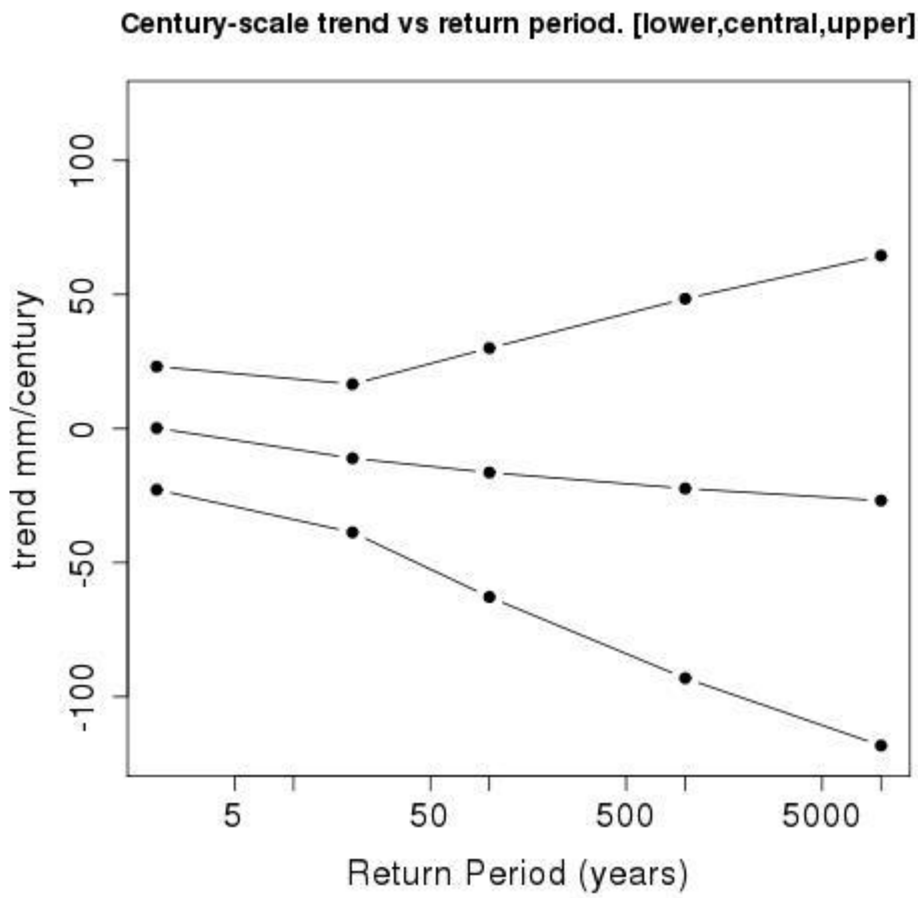

Figure 9.15: Projected century-scale trends in skew surge for five return periods due to storminess changes only (i.e. excluding mean sea level change) (mm per century). Central, lower and upper estimates are shown.

9.4.2 Projections of Extreme Still-Water Level for the 21st Century

In this section we provide a recommended method to combine the sea level projections from Chapter 8 with surge projections from Chapter 9 and existing site-specific return level data, to produce site-specific projections of extreme still water sea level for the 21st Century.

Combined mean sea level and surge projections

Here we combine projections of mean sea level change and projections of change in the extremes due to storminess changes only to give projections of extreme still water level, along with uncertainties. Although the projected changes due to storminess are not statistically significant, we nevertheless use the range of these projections, since this is a component of the uncertainty in the change in extreme sea level.

We take two precautionary steps to avoid underestimation of these uncertainties:

- Uncertainties can be combined in qaudrature (if we are confident that the two sources of uncertainty are independent) or linearly (if we believe that the two sources of uncertainty are correlated). Since we cannot be confident that the two sources are independent, we use linear combination, which gives a more precautionary result.

- The uncertainties in skew surge for a given return period are larger than the uncertainties of the total still water level for the same return period (since total still water level includes the deterministic tide). We take our uncertainties from the skew surge (i.e. the ranges shown in Table 9.2).

It is worth noting that uncertainties in the present-day return levels, which are usually derived from short tide-gauge records, are very likely to be a large component of the combined uncertainty in projected future return-level curves. However we do not advocate using the present model data as a substitute for tide-gauge data in an effort to reduce this component, because of the limitations of the model resolution. Rather, we use the model to tell us about the trends (in both mean and extreme sea level) and the uncertainties in these trends. In order to produce a complete projection of future return levels it will be necessary to combine this uncertainty with the existing uncertainty about present-day return levels derived from tide gauges.

Since the rate of century-scale change in return level of skew surge given in Table 9.2 is by construction linear over time, for the periods of interest (2040, 2070, and 2100) we can simply scale by time from the present day (25 years, 55 years, and 85 years).

Change in mean sea level is discussed in Chapter 8. The relevant mean sea level change projections, derived from information in Chapter 8, are shown in Table 9.3.

Table 9.3 Projected change in mean sea level (metres), derived from information given in Chapter 8

	2040 central [lower upper]	2070 central [lower upper]	2100 central [lower upper]
RCP4.5	0.17 [0.11-0.22]	0.34 [0.20-0.46]	0.51 [0.29-0.73]
RCP8.5	0.18 [0.12-0.23]	0.41 [0.27-0.55]	0.73 [0.46-1.02]

The approach is summarised symbolically below and an example calculation is given.

For RCP8.5:

$$\Delta S_{8,RP} = \Delta Z_8 + \Delta T \frac{dE_{RP}}{dT}$$

Where $\Delta S_{8,RP}$ is the change in extreme still water level under RCP8.5 for return period RP, ΔZ_8 is the change in mean sea level under RCP8.5 for the time window in question, ΔT is the time interval from the present day, and $\frac{dE_{RP}}{dT}$ is the century-scale trend in skew surge for the given return period RP.

Example calculation, RCP8.5:

Suppose we wish to calculate the change by 2070 in the 100-year extreme still water level under RCP8.5.

First for the central estimate:
ΔZ_8= 0.41 m (central estimate, Table 9.3).
ΔT = (2070-2015) years = 55 years = 0.55 century
$\frac{dE_{RP}}{dT}$ = -0.02 m per century (central estimate, Table 9.2, above),
giving $\Delta S_{8,RP}$ = (0.41 +0.55*(-0.02)) m
= 0.40 m

Then for the upper estimate:
ΔZ_8= 0.55 m (upper, Table 9.3).
ΔT = (2070-2015) years = 55 years = 0.55 century
$\frac{dE_{RP}}{dT}$ = 0.03 m per century (upper, Table 9.2, above),
giving $\Delta S_{8,RP}$ = (0.55 +0.55*(0.03)) m
= 0.57 m

And a similar calculation can be made for the lower estimate.

RCP8.5 is expected to give the largest sea level changes among the RCP scenarios used in AR5, and assuming a precautionary approach we have focused our model runs on this scenario. For **RCP4.5** we propose a simple scaling approach for the rate of change in the surge component. We assume the mean sea level change as a crude overall metric of climate change, and use the ratio of the mean sea level change in RCP4.5 to that in RCP8.5 to scale our rate of century-scale change in return level of skew surge from RCP8.5 to RCP4.5.

$$\Delta S_{4,RP} = \Delta Z_4 + \Delta T \frac{dE_{RP}}{dT} \left(\frac{\Delta Z_4^*}{\Delta Z_8^*}\right)$$

Where $\Delta S_{4,RP}$ is the change in extreme still water level under RCP4.5 for return period RP, ΔZ_4 is the change in mean sea level under RCP4.5 for the time window in question, ΔZ_4^* is the central estimate of the change in mean sea level under RCP4.5 for the time window in question, ΔZ_8^* is the central estimate of the change in mean sea level under RCP8.5 for the time window in question and other symbols are as defined above.

Example calculation, RCP4.5:

Suppose we wish to calculate the change by 2070 in the 100-year extreme still water level under RCP4.5.

First for the central estimate:
ΔZ_4 = 0.34 m (central estimate, Table 9.3).
ΔZ_4^*= 0.34 m (central estimate, Table 9.3).
ΔZ_8^*= 0.41 m (central estimate, Table 9.3).
Thus $\left(\frac{\Delta Z_4^*}{\Delta Z_8^*}\right)$ = 0.83

ΔT = (2070-2015) years = 55 years = 0.55 century
$\frac{dE_{RP}}{dT}$ = -0.02 m per century (central estimate, Table 9.2, above),
giving $\Delta S_{8,RP}$ = (0.34 +0.55*(-0.02)*0.83) m
= 0.33 m

Then for the upper estimate:
ΔZ_4= 0.46 m (upper, Table 9.3).
ΔZ_4^*= 0.34 m (central estimate, Table 9.3).
ΔZ_8^*= 0.41 m (central estimate, Table 9.3).
Thus $\left(\frac{\Delta Z_4^*}{\Delta Z_8^*}\right)$ = 0.83
ΔT = (2070-2015) years = 55 years = 0.55 century
$\frac{dE_{RP}}{dT}$ = 0.03 m per century (upper, Table 9.2, above),
giving $\Delta S_{4,RP}$ = (0.46 +0.55*(0.03)*0.83) m
= 0.47 m

And a similar calculation can be made for the lower estimate.

Combining MSL and surge projections with site-specific present-day return level curves

Here we present an example calculation showing how the projections can be combined with present-day return level data to give a projected future return-level. Note however that we have not included any uncertainty in the present-day return levels. In practice that may be a major component of the overall uncertainty, especially for long return periods.

Example calculation:

Suppose we wish to identify the projected 100-year return level of extreme still water under RCP8.5 for the year 2070 at a particular tide gauge location. The change by 2070 in the 100-year extreme still water level under RCP8.5 is given by the example calculation above as 0.4 m (central estimate); 0.57 m (upper estimate) and 0.23 m (lower estimate; this calculation is not shown above but it follows the same procedure as the central and upper calculations. Alternatively, one may note that the ranges are by construction symmetrical, so the lower estimate is given by {0.4 minus (0.57 minus 0.4)} m = 0.23 m).

Suppose we know the present-day 100-year return level of extreme still water at the tide gauge is 2.39 m. We combine this linearly to give the projected 100-year return level of extreme still water under RCP8.5 for the year 2070 at the tide gauge:

Central:	2.39 m + 0.4 m =	2.79 m
Upper:	2.39 m + 0.57 m =	2.96 m
Lower:	2.39 m + 0.23 m =	2.62 m

The projected changes in extreme still water level due to changes in mean sea level and changes in atmospheric storminess (metres) at a point in the Singapore Straits for different return periods are given below for 2050 and 2010 for both RCP8.5 and RCP4.5 are given in Table 9.4.

Table 9.4: Projected changes in extreme still water level due to changes in mean sea level and changes in atmospheric storminess (metres) at a point in the Singapore Straits for different return periods. The lower and upper bounds show a representative range of projections derived by combining mean sea level projections with results from the 4 storm surge simulations, including an estimate of additional uncertainty to compensate for the small ensemble size of surge simulations.

2050 RCP8.5					
Period (years)	2	20	100	1000	10000
Lower Upper	0.16 0.33	0.15 0.33	0.14 0.33	0.13 0.34	0.12 0.34

2100 RCP8.5					
Period (years)	2	20	100	1000	10000
Lower Upper	0.44 1.04	0.42 1.04	0.40 1.05	0.38 1.07	0.35 1.07

2050 RCP4.5					
Period (years)	2	20	100	1000	10000
Lower Upper	0.14 0.30	0.13 0.30	0.12 0.31	0.11 0.31	0.11 0.32

2100 RCP4.5					
Period (years)	2	20	100	1000	10000
Lower Upper	0.29 0.75	0.27 0.75	0.26 0.76	0.25 0.77	0.23 0.78

Summary of results

- Changes in MSL are not included in the tide and surge simulations, but are addressed separately in Chapter 8.
- In the absence of MSL change, the projected trends in the extremes of still water level are small.
- We diagnose trends using two different generalised extreme value models fitted to the largest event each year, one stationary model and one non-stationary.
- In three out of four climate-model simulations the fitted non-stationary GEV model is not significantly better than the stationary GEV model (P-values 9%, 29%, 77%)
- In the fourth model (IPSL) this P-value is less than 1% (i.e. the non-stationary GEV model is significantly better.)
- The IPSL model also differs from the other models in that it projects small decreasing trends.
- Treating the four models as a small ensemble of equally plausible simulations we obtain an ensemble spread of the diagnosed trend in one hundred-year return level of [-63, 30] mm/century (presented as a representative range of the spread). These values are small compared to the uncertainties in projected mean sea-level change, for example [450, 1020] mm over the 21st century (Table 1, Chapter 8).
- We describe how the additional uncertainty in projections of surge extremes can be combined with the uncertainty in mean sea level (described in Chapter 8) to give projected changes in extreme still water level.

9.4.3 Wave Model Results

This section will focus on maps and time series of modelled wave height, comparing results from the historic period (1970-1999) and the end century (2070-2099). A comparison of the 4 different models mean and maximum significant wave height, and maximum wave period can be found in Appendix 9.4.

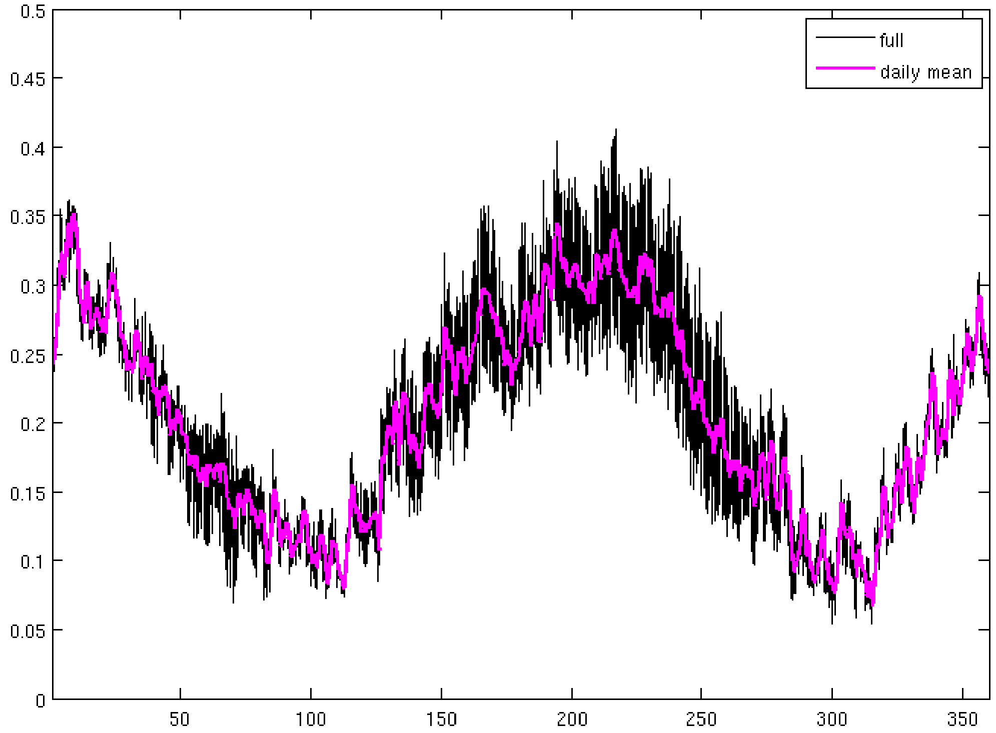

Figure 9.16 Simulated 30-year mean of hourly significant wave heights (metres) close to Singapore during 1970-1999, showing seasonality: large waves during the southwest monsoon (middle year JJA) and also during northeast monsoon (end/start year NDJF). A daily mean is taken (pink line), but large daily variability is observed during the southwest monsoon – caused by land/sea breezes during the Sumatra squalls – see Appendix 9.5

<u>Seasonality and influence of the monsoon</u>

The wave model captures observed seasonality well, with the largest wave heights observed during the two monsoon periods. Figure 9.16 shows the wave height variability at a site close to Singapore, where a 30-year mean is calculated every hour during the simulation. As well as a strong seasonal cycle with wave heights around 25cm larger during the monsoon, shorter term variability is also observed. These faster changes are largest during the southwest monsoon.

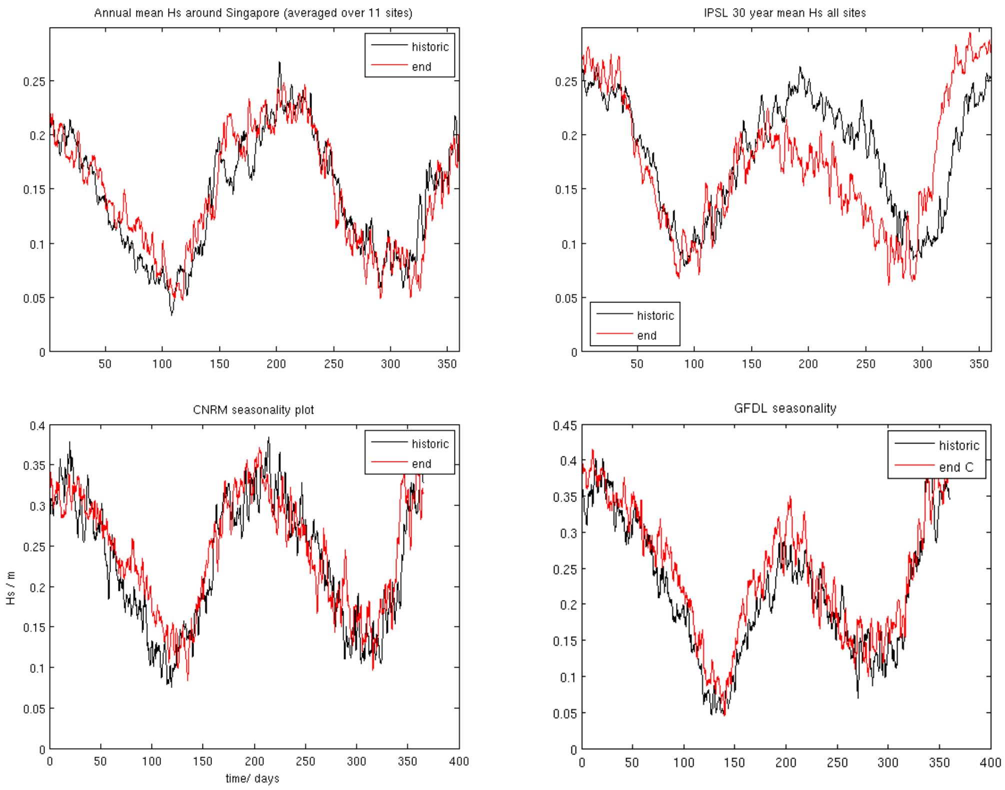

Figure 9.17: Comparing time series of 30-year average significant wave height (metres): historic vs. end century. Top left: HadGEM2-ES; top right: IPSL-CM5A-MR; bottom left: CNRM-CM5; bottom right: GFDL-CM3.

<u>Change in seasonality</u>

Figure 9.17 demonstrates that no clear change in seasonality is observed in HadGEM2-ES. For IPSL-CM5A-MR we see a reduction in strength of the southwest monsoon signal, and a stronger, earlier onset by end century. In the CNRM-CM5 model there is no real change in seasonality or significant wave height. The GFDL-CM3 model sees an increase in mean Hs during the summer period.

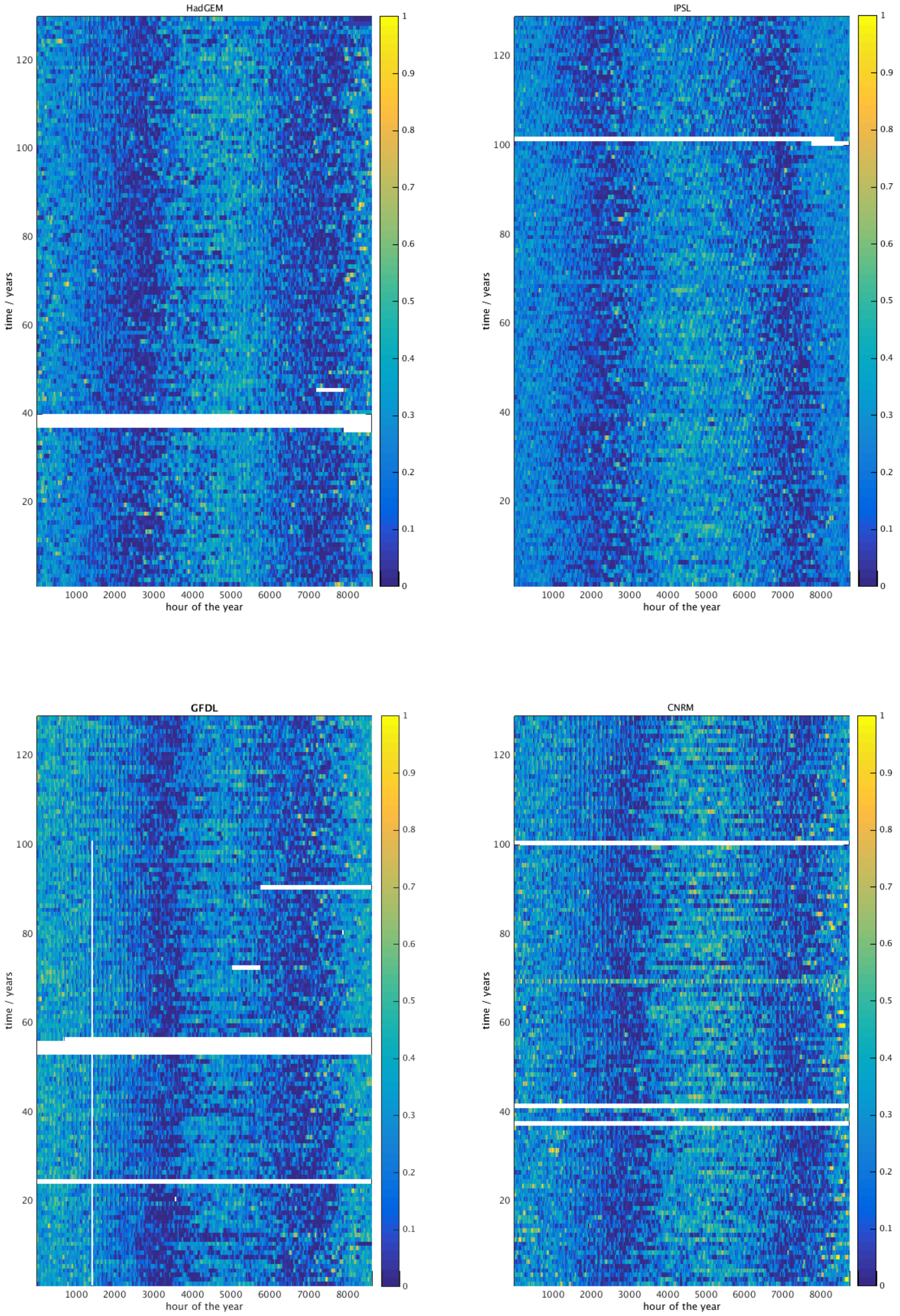

Figure 9.18: Plots showing Hs for HadGEM2-ES (top left) and IPSL-CM5A-MR (top right) GFDL-CM3 (bottom left) and CNRM-CM5 (bottom right). Year up the Y-axis, and day of year on the X-axis. The seasonality stands out as warmer colours during the 2 monsoons, and cooler troughs during the calm periods. Missing data points are left blank.

Long term changes

In order to investigate long term change in wave conditions, Hs was extracted at a single point from each model, and then arranged into a matrix of dimensions (year on the Y-axis by time of year (hour) on the X-axis). The plots in Figure 9.18 then demonstrate a seasonal cycle in the x-direction and interannual variability in the y-direction. For HadGEM2-ES, GFDL-CM3 and CNRM-CM5, no clear change signal is observed moving from the beginning to end of the century. However, for IPSL-CM5A-MR there seems to be a decrease in significant wave heights during summer towards the end of the century. There seems to be an early onset of the northeast monsoon in the IPSL-CM5A-MR data. In the CNRM-CM5 and IPSL-CM5A-MR models, the southwest monsoon looks 'broader' i.e. lasting longer in time than the HadGEM2-ES and GFDL-CM3.

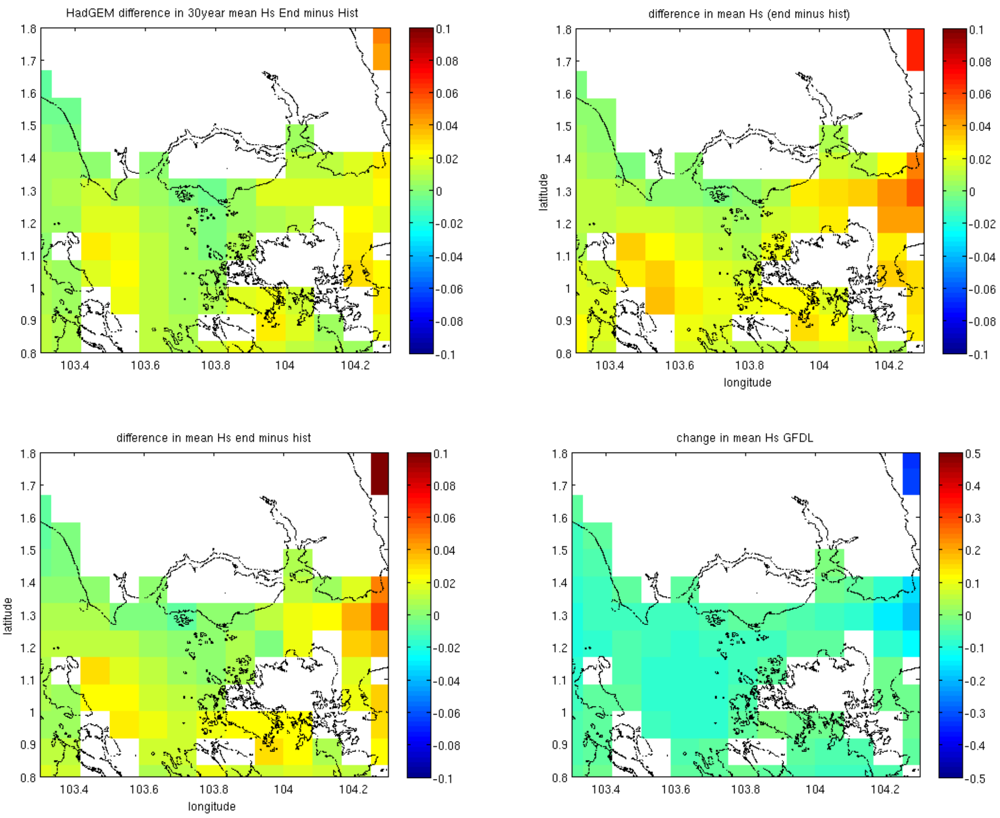

Figure 9.19: Change in mean Hs (metres) from historical to end century, where warmer colours imply larger future waves. (a) HadGEM2-ES, (b) CNRM-CM5, (c) IPSL-CM5A-MR, (d) GFDL-CM3

Changes in 30 year mean wave conditions

This section presents projected changes in mean significant wave height in the 4 different RCMs. Figure 9.20 shows similar maps for the peak wave period, in seconds.

The mean Hs change (Figure 9.19) simulated in HadGEM2-ES, CNRM-CM5, and IPSL-CM5A-MR all show a similar pattern: small changes of the order 5-10 cm, with larger wave heights seen to the east of Singapore. In GFDL-CM3 general decrease in Hs is observed, again of order 10 cm everywhere, this time the largest reduction in wave height is seen to the east, contrary to the other models. However, evaluating the changes in extremes based on individual time slices is problematic, since the signals can be dominated by individual extreme events, so we assess potential changes in the extreme wave climate by considering the long-term trends in the next section.

Differences in peak wave period are presented in Figure 9.20 and can be seen to be of the order +/- 5s. Most models predict a reduction in peak period (i.e. shorter waves), though there is some indication of longer waves approaching the east coast of Singapore, from the South China Sea. These longer period waves are relevant as they can be more energetic, and therefore more damaging.

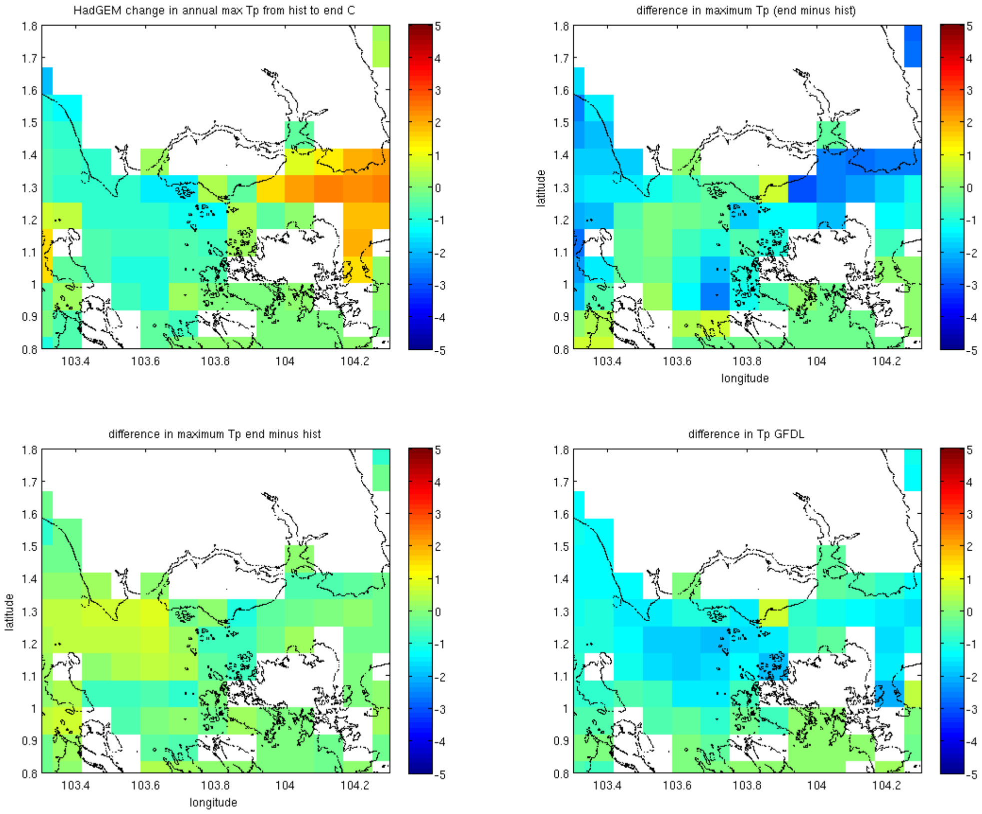

Figure 9.20: Change in maximum peak wave period (seconds) from historical to end century. I.e. hot colours imply longer period future waves, cool colours imply shorter waves. (a) HadGEM2-ES, (b) CNRM-CM5, (c) IPSL-CM5A-MR, (d) GFDL-CM3

Extreme Value Analysis

Our analysis of changes in the extremes of significant wave height follows our approach used for surge. We fit a GEV model to the annual maxima of significant wave height. The degree of improvement in fit as we move to a non-stationary fit measures the statistical significance of the century-scale trends in the extremes for each model. A preliminary analysis of the projections suggests that the greatest inter-model range of century-scale change is found around grid point ‘a’, so we focus on this location. The annual maximum significant wave height at grid point ‘a’ is shown for each of the four simulations in Figure 9.21.

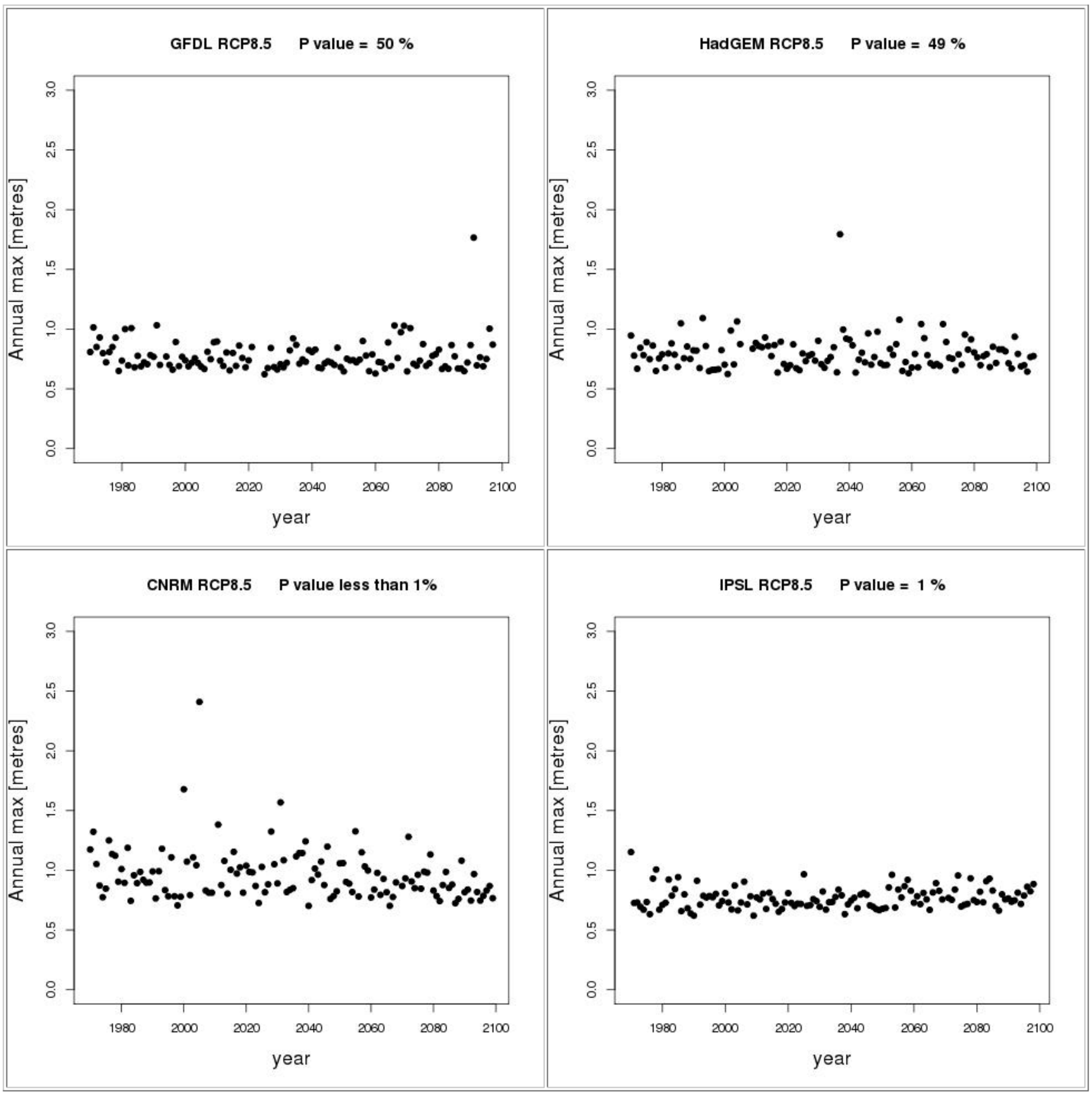

Figure 9.21: Simulated annual maxima of significant wave height (metres). A consistent scale on the Y-axis is used across all four models for ease of comparison. The P-value indicates the statistical significance of the improvement in fit when we use a non-stationary GEV model: large P-value indicates little improvement; small P-value indicates significant improvement. For interpretation of the P-value please see the discussion of the surge projection results in section 9.4.1

All four of the non-stationary fits have a negative trend in the scale parameter. All except IPSL have a negative trend in the location parameter. Thus all of the resulting projections of century-scale trends are negative (except for the IPSL projection of 35 mm/century increase in the 2-year return level). Consistent with our approach to surge changes, we identify an ‘ensemble’ projection, as follows.

For each model, from the non-stationary fit we can diagnose a linear century-scale trend in return level associated with any given return period. In order to produce trends and uncertainties which are representative of the four models taken as a whole, for any given return period we take the four central estimates of trend (one from each model) and identify the mean of these four (μ) as our small-ensemble central estimate and the (Bessel-corrected) standard deviation of these four (σ) as the uncertainty. We then identify (μ - 1.64 σ) as our lower bound and (μ + 1.64 σ) as our upper bound. This is essentially the approach taken in UKCP09 (Lowe et al., 2009) except that Lowe et al. employed a perturbed-physics ensemble with eleven members, whereas we have a multi-model ensemble of only four members. Following this procedure we obtain century-scale trends as shown in Table 9.5. These values are illustrated in Figure 9.22. For other return periods, interpolation between the points in Figure 9.22 is acceptable.

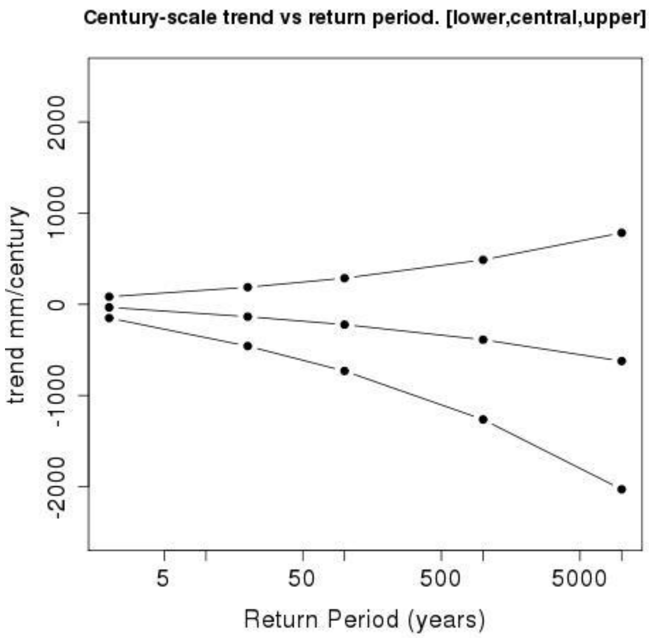

Figure 9.22: Projected century-scale trends in significant wave height for five return periods due to storminess changes (mm per century). Central, lower and upper estimates are shown.

Table 9.5: Projected century-scale trends in significant wave height for five return periods due to storminess changes (metres per century, to two decimal places)

Period/years	2	20	100	1000	10000
Lower	-0.15	-0.46	-0.73	-1.26	-2.03
Central	-0.03	-0.14	-0.22	-0.39	-0.62
Upper	0.08	0.19	0.29	0.49	0.78

The uncertainty in projected trends in significant wave height for long return periods shown in Table 9.5 is not small in the context of the uncertainties in mean sea level change. This is a reflection of the large uncertainties inherent in levels associated with long return periods: these are essentially extrapolations from the available data. It should be noted however that in all four models the central projection is for a decrease in the levels associated with long return periods; the possible increases at long return periods indicated by the ‘upper’ line in Figure 9.22 (‘upper’ row in Table 9.5) are a result of our identification of ($\mu + 1.64\ \sigma$) as our upper bound. Figure 9.23 shows Figure 9.22 replotted with the central estimates from each model also shown. It can be seen here that we do not have any evidence within our four simulations of positive trends in the long-return-period levels, but the variation between models suggests that such positive trends might be found if further CMIP models could be tested. Thus the inclusion of further CMIP models is highly desirable in any future work.

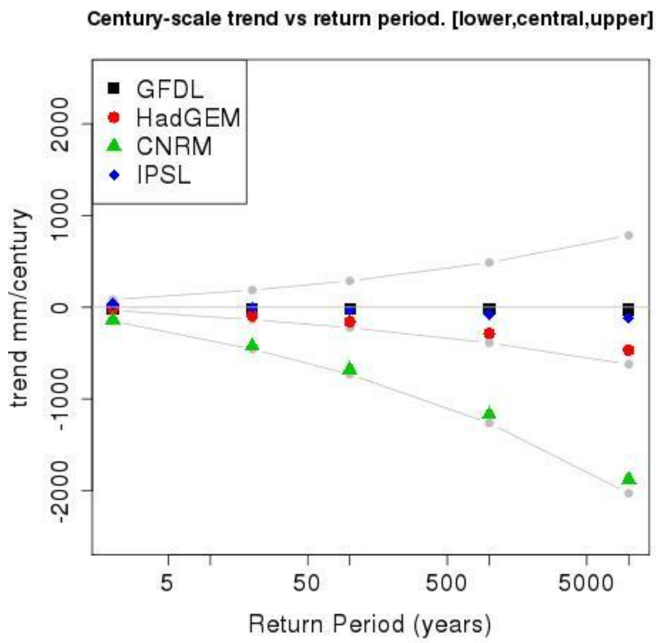

Figure 9.23: As Figure 9.22, with central estimate from each model (coloured markers and with zero-trend line) also shown. Note that none of the four models project a positive trend in long-return-period levels.

9.5. Summary

Our primary finding is that projected changes in mean sea level dominate over projected changes in surge or waves, at least for short return periods (say, less than 5 years) where the findings are more robust. This result – that projected changes are dominated by projected MSL changes – echoes results found in other regional studies, for example Lowe et al., 2009. For long return periods the uncertainty in projections of change in waves is very large, but this is just a reflection of the inherent uncertainty in dealing with long return periods. Our lower and upper estimates for changes in surge and waves represent a range of projections derived from the 4 models, including an estimate of additional uncertainty to compensate for the small ensemble size compared with the atmospheric projections.

Taking the four climate models as a whole we find no statistically significant changes in extreme skew surge events and no statistically significant changes in extreme significant wave height. The inter-model spread of century-scale change in levels associated with short return periods in either surge or waves is small compared to uncertainties in mean sea level change. For example, for RCP8.5 to 2100 we project changes in the range [-20, 20] mm/century in 2-year return level of skew surge, and [-150, 80] mm/century in 2-year return level of significant wave height, compared to a change in the range [460, 1020] mm in mean sea level. For surges this is also true for long return periods (for example [-120, 60] mm/century change in ten thousand-year return level of skew surge). For waves, our metric of inter-model spread of century-scale change in levels associated with *long* return periods is *not* small (e.g. [-2030, 780] mm/century change in ten thousand-year return level of significant wave height). This large spread is a result of the inevitable uncertainty in levels associated with long return periods. However it should be noted that the central estimate of the trend in these long return levels is negative in each of the individual models. The positive values quoted are a result of compensating for the small sample size of four. This provides a strong argument for using a larger ensemble wherever possible in future work.

Our wave modelling successfully simulates the seasonal signal in wave height associated with the monsoons, with the largest modelled wave heights seen during the northeast monsoon (Dec-Feb) and a second peak during the southwest monsoon (Jun-Aug). We note that the waves are typically more damaging during the winter season due to sea level set-up. There is some evidence of a projected change in wave seasonality but this is not reflected in a statistically significant trend in significant wave height.

9.6. Interpretation and Limitations

Analysis of the individual components of changes in extreme sea level for Singapore has led to a recommended method to combine mean sea level projections with surge projections, and present-day site-specific data, to generate site-specific projections of extreme sea level through the 21st Century with associated estimates of uncertainty. The method is detailed in Section 9.4.2, and we provide sample calculations there and in Appendix 9.9.

Our method takes into account what we consider most likely to be the dominant drivers of extreme sea level change for Singapore, and provides formal uncertainty estimates on the projections which we consider to be 'state of the art'. The approach is broadly similar to that used for the most recent UK sea level projections (Lowe et al. 2009). However there remain a number of more structural/methodological uncertainties, and scope for future refinement. Here we aim to provide context by considering the limitations of our 'worst case' projections for changes in 100 year site-specific return levels for 2100 under RCP8.5. These are summarised in the bullets below, and a more detailed discussion of each term is presented in Subsection 9.6.1. The projections are made up of the following terms:

- *Changes in mean sea level*: **102 cm** plus poorly constrained risk from Antarctic ice sheet (unlikely, not exceeding 'several tenths of a metre')
- *Changes in skew surge*: **3 cm.** A number of terms are not considered, e.g**.** wave-surge interaction, propagation of surge from outside model domain, changes in seasonality, and changes in tropical cyclones. However these are unlikely to exceed the magnitude of the current surge estimate.
- *Changes in large scale climate variability*. For La Nina this is expected to contribute **less than 1 cm**.

- *Uncertainty in estimates of current return levels*: may lead to an increase in the upper bound for *both* the current *and* the 2100 return levels. As far as we are aware this uncertainty is currently **unquantified**.
- *Changes in spatial structure of mean sea level and surge around Singapore*. Not fully quantified but changes in tidal resonance may contribute of order **5 cm**.

Given the above, we judge that the four greatest uncertainties in our current upper projection of extreme sea level change (greatest first) arise from:

1. Uncertainty in the mean sea level term, especially that arising from possible Antarctic Ice Sheet changes
2. Currently unquantified uncertainty in estimates of present day return levels
3. Possible changes in the detailed spatial structure of mean sea level and surge around Singapore
4. Effects of possible *changes* in large scale modes of climate variability

Of these, (1) is a long term, global research problem; (2) may be tractable through a combination of observations and models/reanalyses, and (3) is likely tractable through a two-stage downscaling approach (global models → SE Asian shelf seas → Singapore region); and (4) requires first a deeper study of projected changes in regional climate variability in global climate models. We suggest that (1)-(4) would be priority topics for any future research on extreme sea level for Singapore.

9.6.1 Detailed discussion of uncertainties

This subsection presents supporting discussion of the key uncertainties described above. Where numerical values are given they are related to our upper estimates of site-specific 100-year return height, using the methods of Section 9.4.

- *Changes in mean sea level:* The mean sea level term is presented as a *likely* range (66-100% probability), based on the expert judgement of the IPCC AR5 authors taking into account a number of uncertainties that cannot be formally quantified with the present state of scientific knowledge. The most important of these is the unknown (but thought to be unlikely) probability of Antarctic ice sheet collapse. The assessment of AR5 was that if this were to occur, the resultant additional global sea level rise would not exceed "several tenths of a metre" during the 21st Century. One would expect this to be scaled up by a further factor for the mean sea level rise at Singapore (a factor of 1.19 was used in Chapter 8). This remains one of the most important structural uncertainties in projecting sea level extremes. While it is not currently possible to formally quantify these uncertainties beyond the above statement, a precautionary approach to risk management might consider taking them into account, for example by adding an increment to the model-derived upper bound.

- *Skew surge changes (i):* Surge propagation from outside the boundaries of the surge model domain is not considered (except by application of a static inverse barometer effect at the boundaries). However, over shallow seas the wind is the dominant factor in surge generation, so we anticipate that propagation from outside the boundaries will not be an important effect (K. Horsburgh, pers. comm.).

- *Skew surge changes (ii):* Our regional climate model may not have sufficient resolution to simulate a realistic central pressure in tropical cyclones (Chapter 5). However, as discussed in the introduction, tropical cyclones are thought unlikely to be an important factor for extreme sea level in Singapore.

- *Skew surge changes (iii):* Time series of simulated surge and tide water levels provided on the data portal could be used to assess changes in the seasonality of surge, which has not been considered in this work.

- *Changes in large scale patterns of interannual climate variability:* For example the El Nino Southern Oscillation, the Madden Julian Oscillation, Indian Ocean Dipole. Changes in these modes were not considered explicitly in this study. It is known that La Nina events favour high time-mean sea level anomalies of order 5 cm (Tkalich et al. 2013), which would be expected to increase the probability of extreme high sea level during La Nina. Our recommended method to generate site-specific projections involves adding projected changes in multi-year-mean sea level and surge statistics (single values for all Singapore) to present-day site-specific return curves derived from observations. The present day site-specific return curves already include the effects of present-day climate variability (albeit with some uncertainty due to limited time series – see next bullet). So the only term missing comes from possible changes in variability (e.g. in ENSO amplitude). IPCC AR5 concludes that confidence in projected ENSO changes is low, with the multi-model mean of model simulations indicating an increase in variability of less than 10% for RCP8.5 (Christensen et al. 2013). Using Tkalich et al's (2013) figure, this might be expected to result in an increase of less than 0.5 cm in extreme sea level anomalies at all return periods, which is small compared with other sources of uncertainty. Nonetheless the impacts of changes in key modes of climate variability remain a significant source of modelling uncertainty and a fuller study of the effects of changes in large scale climate drivers would be valuable.

- *Uncertainty in estimates of current return levels:* Estimates of current return levels based on tide gauge data are liable to suffer from substantial uncertainty due to the limited length of timeseries available. For example the impact of a relatively rare (say 1 in 20 year) surge might be expected to be greater if it occurred during a La Nina event, yet such a coincidence might not be seen during a tide gauge timeseries of a few decades. We therefore consider it likely that uncertainties in extreme still water levels will be a major component of the uncertainty in projected future extreme still water levels. The skew surge joint probability method (Batstone et al., 2013) provides an approach to this problem. In the longer term, the increasing use of long historical simulations/reanalyses suggests there is potential to develop better estimates of current risk by combining model-derived information with observed time series.

- *Changes in spatial structure of extremes (i):* Projected changes in mean sea level and surge both have very large spatial scales compared with the scale of Singapore (see for example Figures 8.1-8.3, 8.5, 9.11). Therefore changes in extreme sea level are expected to be approximately uniform around Singapore. Local effects could result in some spatial variation in how the large scale changes are felt at different locations in Singapore. This could be addressed in principle by a high resolution, second level of downscaling.

- *Changes in spatial structure of extremes (ii):* One process not considered is the impact of changes in mean water depth on tidal resonance and on surge propagation. Pickering (2014) performed sensitivity experiments, raising global MSL by 2 m (greater than our largest projected change) with fixed coastlines, and found a change in mean high water level of the order 10 cm around Singapore. This suggests that tidal resonance effects will be small (order 5 cm), compared to MSL rise. For NW Europe, Howard et al. (2010) find that changing the water depth does not alter the final water level, but only affects the time of arrival of storm surge. This reflects the findings of other workers (e.g. Sterl et al., 2009; Lowe et al., 2001).

- *Changes in spatial structure of extremes (iii):* Our simulations assume a fixed coastline with no inundation. This is probably a reasonable approximation on the scales we are currently modelling at, but if a very high resolution local scale model were used in future this would become more important. A version of the NEMO model which allows ‘wetting and drying’ of coastal gridpoints is currently under development.

- *Waves:* The small sample size (four climate models) and the large spread in projections of century-scale change in significant wave height at long return periods means that we cannot rule out positive trends, even though such the central estimates of the trends are negative in each of the four models. Thus it is very desirable to test further members of the CMIP ensemble in any future work, in order to find out whether such positive trends are in fact realised by any member.

- *Waves:* The wave model is very sensitive to the water depth, and ‘deep’ points may behave very differently to ‘shallow’ points, even though both are close to the coast. Figure 9.2 shows the model bathymetry close to Singapore, which should be considered in conjunction with the projected significant wave heights. The wave results from this study would need to be combined with the tide and surge water levels through an overtopping model to assess coastal risk more comprehensively, but this was beyond the scope of this study.

Acknowledgements

We would like to thank Clare Bellingham, Clare O'Neill, Chris Bunney, Jonathan Tinker, Andy Saulter, and James Harle for their technical work with the configuration and help with running of the wave and surge models.

We wish to acknowledge the help given freely by experts including Professor Jonathan Tawn of Lancaster University and Dr Kevin Horsburgh and Professor Judith Wolf of National Oceanography Centre, Liverpool. Their advice has been invaluable in formulating our approach. However this should not be taken to imply that our approach is necessarily endorsed by these experts.

References

Atlas, R., R. N. Hoffman, J. Ardizzone, S. M. Leidner, J. C. Jusem, D. K. Smith, D. Gombos, 2011: A cross-calibrated, multiplatform ocean surface wind velocity product for meteorological and oceanographic applications. Bull. Amer. Meteor. Soc., 92, 157-174. doi: 10.1175/2010BAMS2946.1

Batstone, Crispian; Lawless, Mark; Tawn, Jonathan; Horsburgh, Kevin; Blackman, David; McMillan, Alastair; Worth, David; Laeger, Stefan; Hunt, Tim. 2013 A UK best-practice approach for extreme sea-level analysis along complex topographic coastlines. Ocean Engineering, 71. 28-39. 10.1016/j.oceaneng.2013.02.003

Bidlot, J.R., Holmes-Bell, D.J., Wittmann, P.A., Lalbeharry, R., Chen, H.S., 2000. Intercomparison of the performance of operational ocean wave forecasting systems with buoy data. European Centre for Medium-Range Weather Forecasts (ECMWF) Technical Memorandum Number 315 also 2002, Weather and Forecasting, 17, 287-310.

Bidlot J-R, J-G Li, P Wittmann, M Fauchon, H Chen, J-M Lefevre, T Bruns, D Greenslade, F Ardhuin, N Kohno, S Park and M Gomez, 2007: Inter-comparison of operational wave forecasting systems. 10th International Workshop on Wave Hindcasting and Forecasting and Coastal Hazard Symposium, North Shore, Oahu, Hawaii, 11-16 November 2007.

Bidlot J.-R. and M.W. Holt, 2006: Verification of operational global and regional wave forecasting systems against measurements from moored buoys. JCOMM Technical Report, 30. WMO/TDNo.1333.

Butler, A., Heffernan, J.E., Tawn, J.A., Flather, R.A. and Horsburgh, K.J. (2007) Extreme value analysis of decadal variations in storm surge elevations. Journal of Marine Systems67 pp189-200

Christensen, J.H., K. Krishna Kumar, E. Aldrian, S.-I. An, I.F.A. Cavalcanti, M. de Castro, W. Dong, P. Goswami, A. Hall, J.K. Kanyanga, A. Kitoh, J. Kossin, N.-C. Lau, J. Renwick, D.B. Stephenson, S.-P. Xie and T. Zhou, 2013: Climate Phenomena and their Relevance for Future Regional Climate Change. In: Climate Change 2013: The Physical Science Basis. Contribution of Working Group I to the Fifth Assessment Report of the Intergovernmental Panel on Climate Change [Stocker, T.F., D. Qin, G.-K. Plattner, M. Tignor, S.K. Allen, J. Boschung, A. Nauels, Y. Xia, V. Bex and P.M. Midgley (eds.)]. Cambridge University Press, Cambridge, United Kingdom and New York, NY, USA.

Coles, Stuart. An introduction to statistical modeling of extreme values. pp 208. London: Springer, 2001.

de Vries, et al., 1995: A comparison of 2D storm-surge models applied to three shallow European seas. Environmental Software, 10(1), 23-42.

Embrechts, P., C. Klüppelberg, and T. Mikosch. Modelling Extremal Events for Insurance and Finance. New York: Springer, 1997.

Frank Farquharson, Fai Fung, Jahir U. Chowdhury, Ahmadhul Hassan, Kevin Horsburgh, Jason Lowe and Tom Howard (2007) “Department for International Development KAR Project R8038 Impact of CLimate And Sea Level Change in part of the Indian Sub-Continent (CLASIC) Final Report”

Holland, Greg J., Amanda H. Lynch, and Lance M. Leslie. "Australian east-coast cyclones. Part I: Synoptic overview and case study." Monthly Weather Review 115.12 (1987): 3024-3036. Hosking, J. R. M., James R. Wallis, and Eric F. Wood. "Estimation of the generalized extreme-value distribution by the method of probability-weighted moments." Technometrics 27.3 (1985): 251-261.

Howard, Tom, Jason Lowe, and Kevin Horsburgh. "Interpreting century-scale changes in southern North Sea storm surge climate derived from coupled model simulations." *Journal of Climate* 23.23 (2010): 6234-6247.

Huerta, Gabriel, and Bruno Sansó. "Time-varying models for extreme values." Environmental and Ecological Statistics 14.3 (2007): 285-299.

Kotz, S., and S. Nadarajah. Extreme Value Distributions: Theory and Applications. London: Imperial College Press, 2000.

Lowe, JA et al. UK Climate Projections Science Report: Marine and Coastal Projections 85–90 (Met Office Hadley Centre, Exeter, UK, 2009);

Lowe, JA., J. Gregory, and R. Flather, 2001: Changes in the occurrence of storm surges around the United Kingdom under a future climate scenario using a dynamic storm surge model driven by the Hadley Centre climate models. Clim. Dynam., 18 (3-4), 179–188.

Maren, D. S., and H. Gerritsen. "Residual flow and tidal asymmetry in the Singapore Strait, with implications for resuspension and residual transport of sediment." *Journal of Geophysical Research: Oceans (1978–2012)* 117.C4 (2012).

Madec G. 2008: "NEMO ocean engine". Note du Pole de modélisation, Institut Pierre-Simon Laplace (IPSL-CM5A-MR), France, No 27 ISSN No 1288-1619.

McSweeney, C., Rahmat, R., Redmond, G., Marzin, C., Murphy, J., Jones, R., Cheong, W.K., Lim, S.Y. and Sun, X. (2013), Sub-selection of CMIP5 GCMs for downscaling over Singapore. Met Office V2 Stage 2 Science Report. 90pp (Chapter 3).

Mínguez, R., et al. "Pseudo-optimal parameter selection of non-stationary generalized extreme value models for environmental variables." Environmental Modelling & Software 25.12 (2010): 1592-1607.

Monbaliu, Jaak, et al. (2000) "The spectral wave model, WAM, adapted for applications with high spatial resolution." *Coastal engineering* 41.1 41-62.

Palmer, M., K. McInnes and M. Chattopadhyay (2014a), Key factors for sea level rise in the Singapore region. Met Office V2 Stage 5 Science Report. 23pp (see Chapter 8).

Palmer, M., D. Calvert, T. Howard, J. Krijnen and C. Roberts (2014b), Summary Report on Changes in Extreme Water Levels in Singapore Region: Part A - Time Mean Sea Level. Met Office V2 Stage 5 Science Report. 34pp.(see Chapter 8)

Pawlowicz, R., B. Beardsley, and S. Lentz, "Classical Tidal Harmonic Analysis Including Error Estimates in MATLAB using T_TIDE", Computers and Geosciences, 28, 929-937 (2002)

Pickering, Mark (2014) The impact of future sea-level rise on the tides. *University of Southampton, Ocean and Earth Science, Doctoral Thesis* , 347pp.

Sterl, A., H. van den Brink, H. de Vries, R. Haarsma, and E. van Meijgaard, 2009: Anensemble study of extreme North Sea storm surges in a changing climate. Ocean Sci., 5, 369–378.

Tawn, J. A. (1992). Estimating probabilities of extreme sea-levels, Appl. Statist., 41, 77-93.

Tkalich, P., Vethamony, P., Luu, Q.-H., and Babu, M. T. (2013), Sea level trend and variability in the Singapore Strait, Ocean Sci., 9, 293-300, doi:10.5194/os-9-293-2013.

Tolman, H. L., 1997: User manual and system documentation of WAVEWATCH-III version 1.15. NOAA / NWS / NCEP / OMB Technical Note 151, 97 pp.

Tolman, H. L., 1999a: User manual and system documentation of WAVEWATCH-III version 1.18. NOAA / NWS / NCEP / OMB Technical Note 166, 110 pp.

Tolman, H. L., 2009: User manual and system documentation of WAVEWATCH III version 3.14. NOAA / NWS / NCEP / MMAB Technical Note 276, 194 pp.

Tolman, H.L. and D.V. Chalikov, 1996. Source terms in a 3rd generation wind-wave model. J. Phys. Oceaonogr., 26, 2497-2518.